BETA-GA_2O_3: A TRANSPARENT CONDUCTIVE OXIDE FOR POTENTIAL RESISTIVE SWITCHING APPLICATIONS

Xiaohao Zheng

A dissertation

submitted in partial fulfillment of the

requirements for the degree of

Doctor of Philosophy

University of Washington

2016

Reading Committee:

Fumio Ohuchi, Chair
Marjorie Olmstead
Alex Jen

Program Authorized to Offer Degree:

Material Science and Engineering

University of Washington

Abstract

BETA-GA_2O_3: A TRANSPARENT CONDUCTIVE OXIDE FOR POTENTIAL RESISTIVE SWITCHING APPLICATIONS

Xiaohao Zheng

Chair of the Supervisory Committee:
Fumio Ohuchi
Material Science and Engineering

My primary research focus is controlling conductivity in Ga_2O_3, with the broader goal of seeking both new materials science and possible applications. Regarding new materials science, the key goal is to elucidate connections between defects and conductivity in β- Ga_2O_3, then, based on an understanding of the conduction mechanism of Ga_2O_3, determine and evaluate the potential of β-Ga_2O_3 as a resistive switching (RS) material.

To systematically investigate the feasibility of Ga_2O_3 in memristor applications, several aspects was examined.

One of the first questions to be answered is how defects play a role in the conductivity of Ga_2O_3. To establish connections between conductivity and defects, a direct approach is to

investigate the connections between the local structure and the concomitant electronic responses, paying particular attention to the role of both intrinsic and extrinsic defects. The approach I used was to compare the directional and thermal dependence of the conductivity induced through annealing in various environments (i.e., intentionally changing the intrinsic and extrinsic defect concentrations), and elucidate the roles of dimensionality and sample processing in controlling these processes through a comparison of the bulk. Such a strategy involves careful characterization of both the atomic and electronic structure at both nanoscopic and macroscopic length scales. Although various calculations has predicted conductivity is independent from oxygen vacancy, no experimental work is reported as supports to theoretical studies due to the hardness to dissociate oxygen vacancy increase from other defect changes, such as Hydrogen interstitial increase, surface band bending reduction from surface population of charged vacancies, metal contact to Ga_2O_3 interface changes, etc . We intentionally inject and/or remove oxygen defects through annealing in oxidizing and reducing atmospheres. The effects of such annealing treatments were investigated using X-ray photoelectron spectroscopy (XPS), scanning tunneling microscopy (STM), and a physical property measurement system (PPMS) to determine chemical and electronic structure, surface characteristics, and transport properties, respectively.

Next, we want to determine the most efficient way to induce a defect concentration change. Electrical field-induced redox reactions and thermal power-induced defect migration are two major driving forces of current RS materials. In this case, I employed two approaches when annealing samples: applying a direct current to the sample, which subjects the material to both an electric field and an elevated temperature, and thermally heating the sample using a resistive heating block. The contribution of contact to Ga_2O_3 interfaces are also intensively investigated, opposed to in

single crystal study, experiments were designed to avoid contact uncertainties. Changes in the conductivity were subsequently examined by electrical measurements.

By seeking answers to the above questions, we found evidences to defect agglomerations, likely Ga vacancies, in single crystal Ga_2O_3 and determined its potentials to be controlled thermally and electrically. As a result, we can switch bulk single crystal Ga_2O_3 between high conductivity and low conductivity states.

To realize this resistive switching behavior in a device, a set of experiments to synthesize Ga_2O_3 films with desired properties and optimize both the device geometry and contact conditions was conducted. A subsequent investigation into device performance and analyses of the structural and interfacial characteristics of the devices was performed.

Thus, this thesis aims to answer three major questions, two of which relate to the intrinsic properties of Ga_2O_3 and one that is associated with device fabrication and characterization. In this report, common "to understand" and "to utilize" strategies were followed to address Ga_2O_3 resistive switching in two parts: Ga_2O_3 material investigation and Ga_2O_3 resistive switching applications.

TABLE OF CONTENTS

LIST OF FIGURES

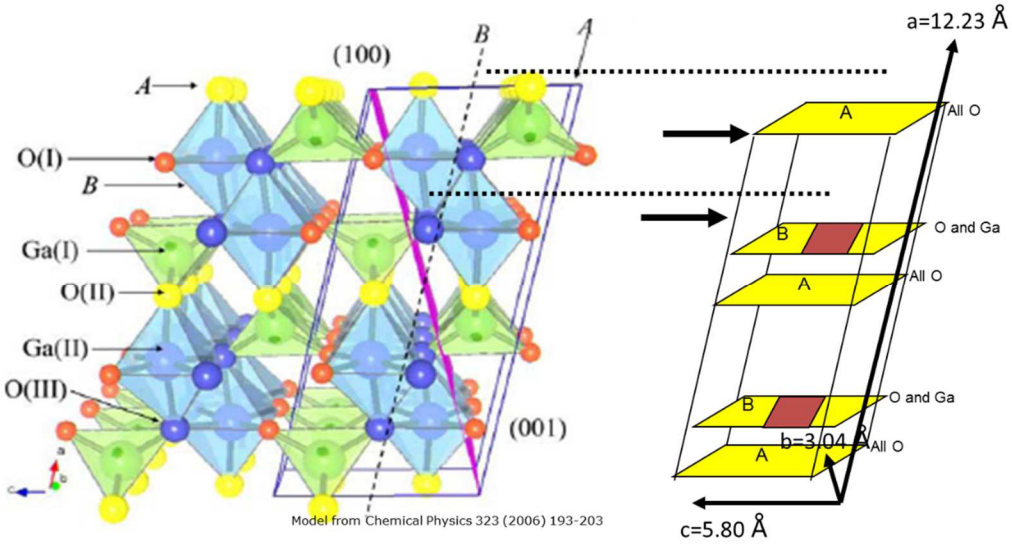

Fig. 1. β- Ga_2O_3 crystal structure[1] showing tetrahedral (I) and octahedral (II) Ga sites, 3-fold (I and III) and 4-fold coordinated O sites, and open channels in the b-direction (Perpendicular to page).

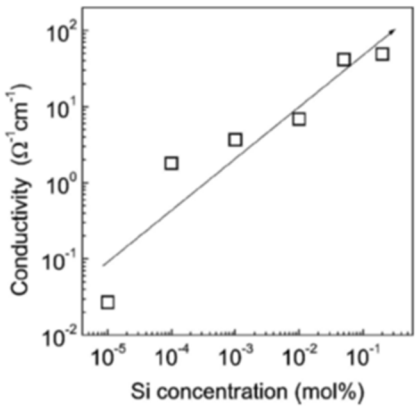

Fig.2. Conductivity of β- Ga_2O_3 as a function of Si impurity concentration[2]

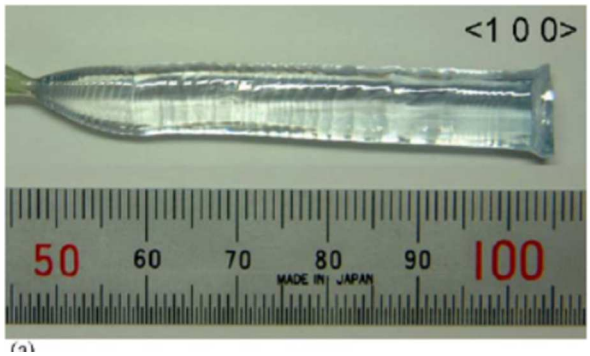

Fig.3. Single crystal beta- Ga_2O_3 grown by the float zone technique at the National Institute for Materials Science.

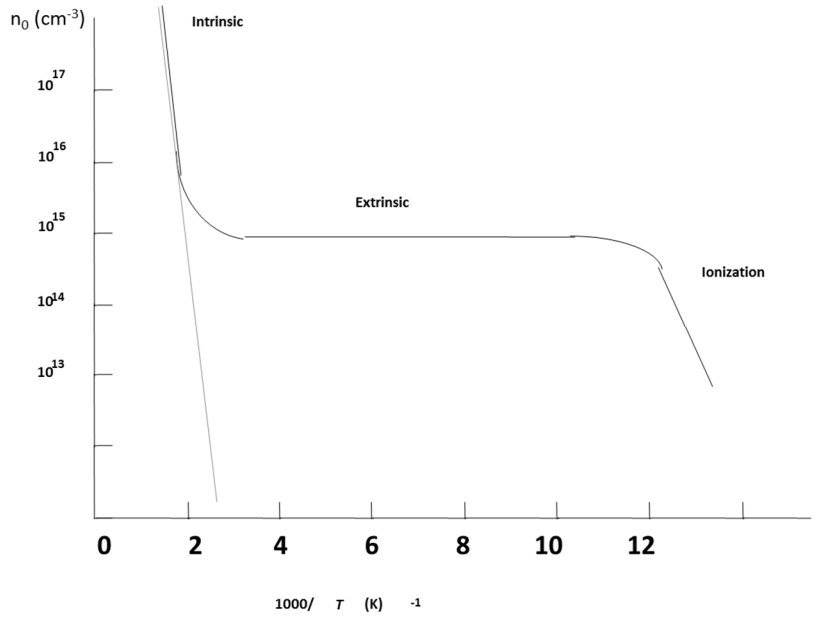

Fig.4. Number of charge carriers found in the conduction band as a function of temperature in conventional doped semiconductors.

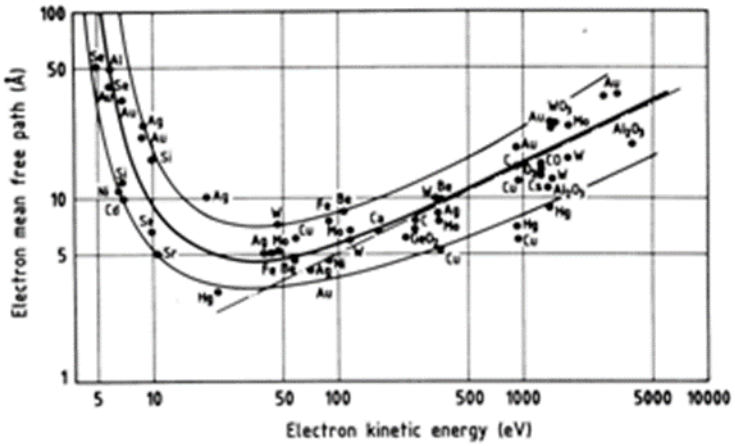

Fig.5. Electron mean free path (Å) vs electron kinetic energy (eV)

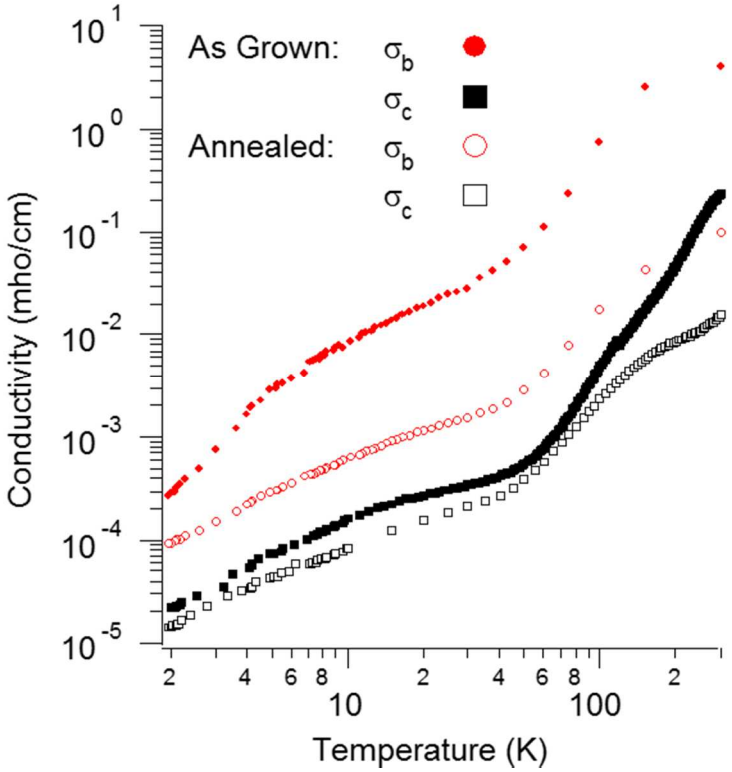

Fig. 6. Electrical conductivity versus temperature plot in double log-scale; "As-grown" and "as-annealed" (600 °C in $1x10^{-8}$ Torr) samples were measured in both the b- and c-directions.

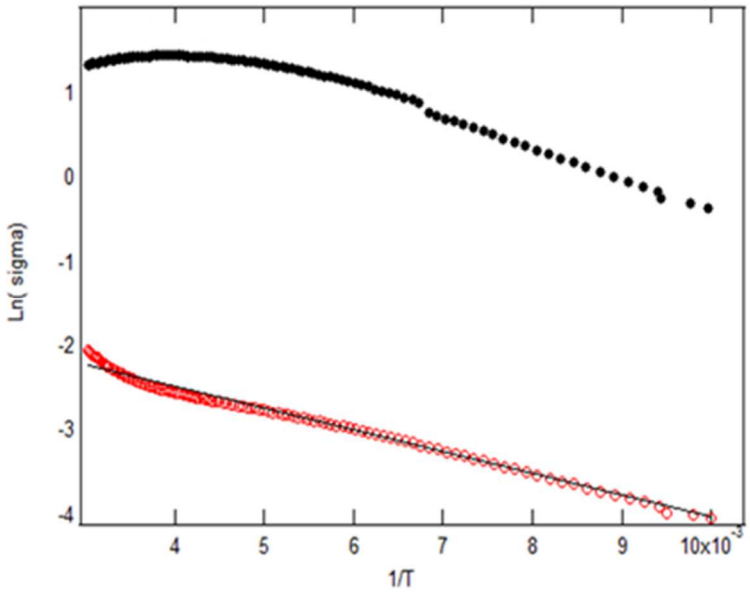

Fig.7. Arrhenius plot above 50K

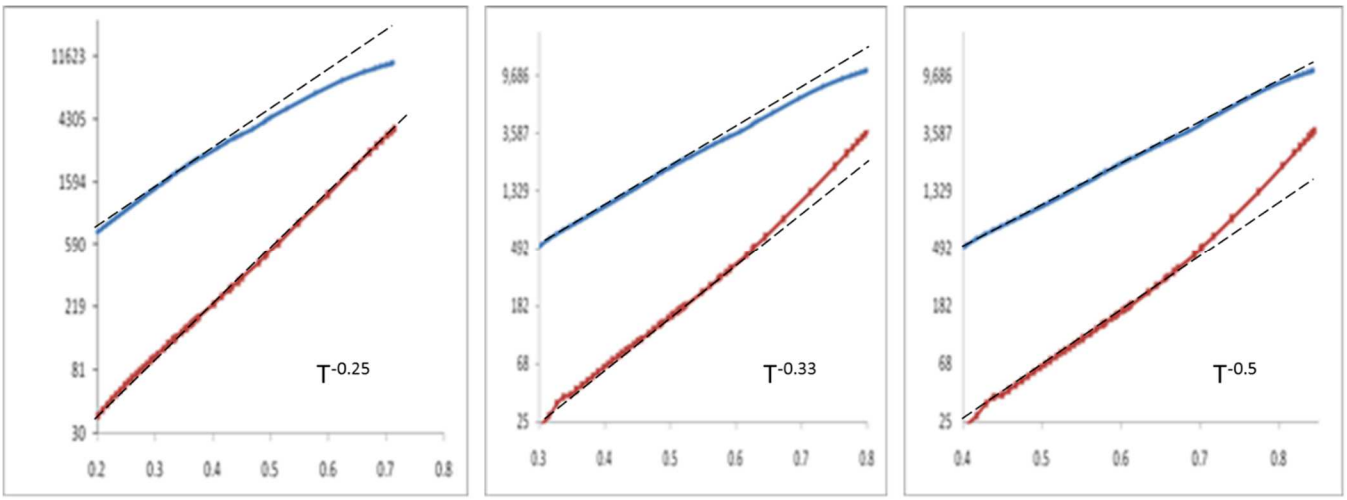

Fig.8. Tm trend of <50 K data, blue line is as grown sample, showing linear trend to $T^{-0.5}$, Red line is annealed sample, showing linear trend to $T^{-0.25}$

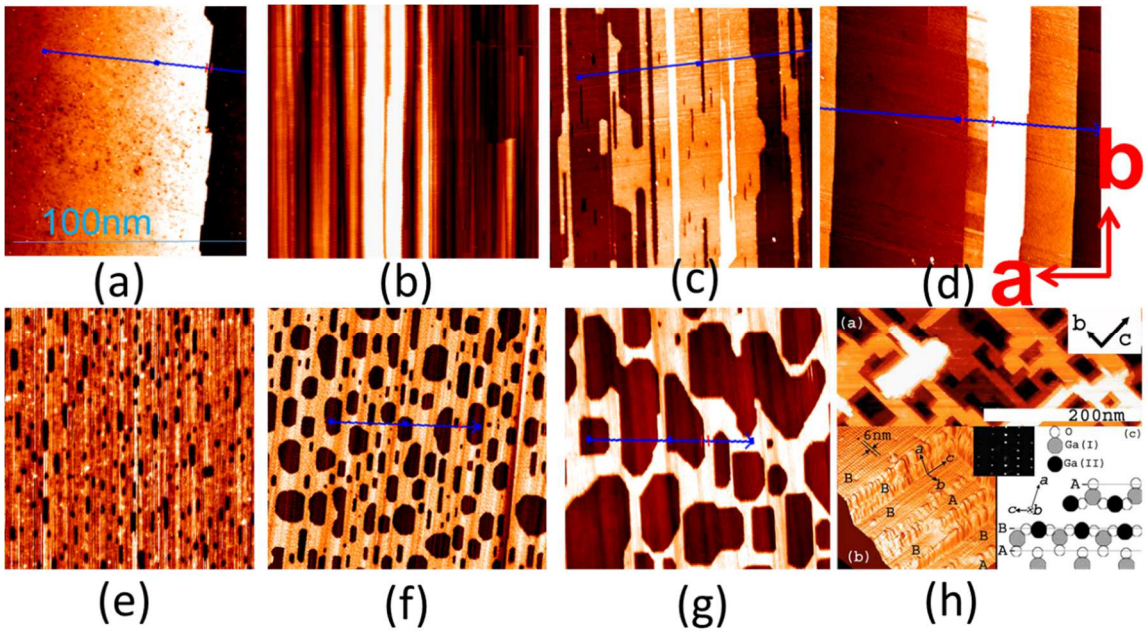

Fig.9. STM scan of β- Ga_2O_3 with increasing annealing time. From left to right are after 4sec, 17sec, 45sec, 180sec, 7200 sec and 20 hours, h) figure from [3].

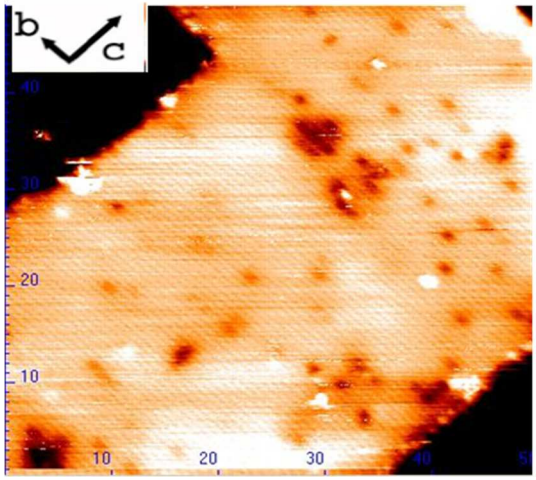

Fig. 10. Atomic Resolution STM on beta- Ga_2O_3 sample post 1100 Degree C anneal for 30min

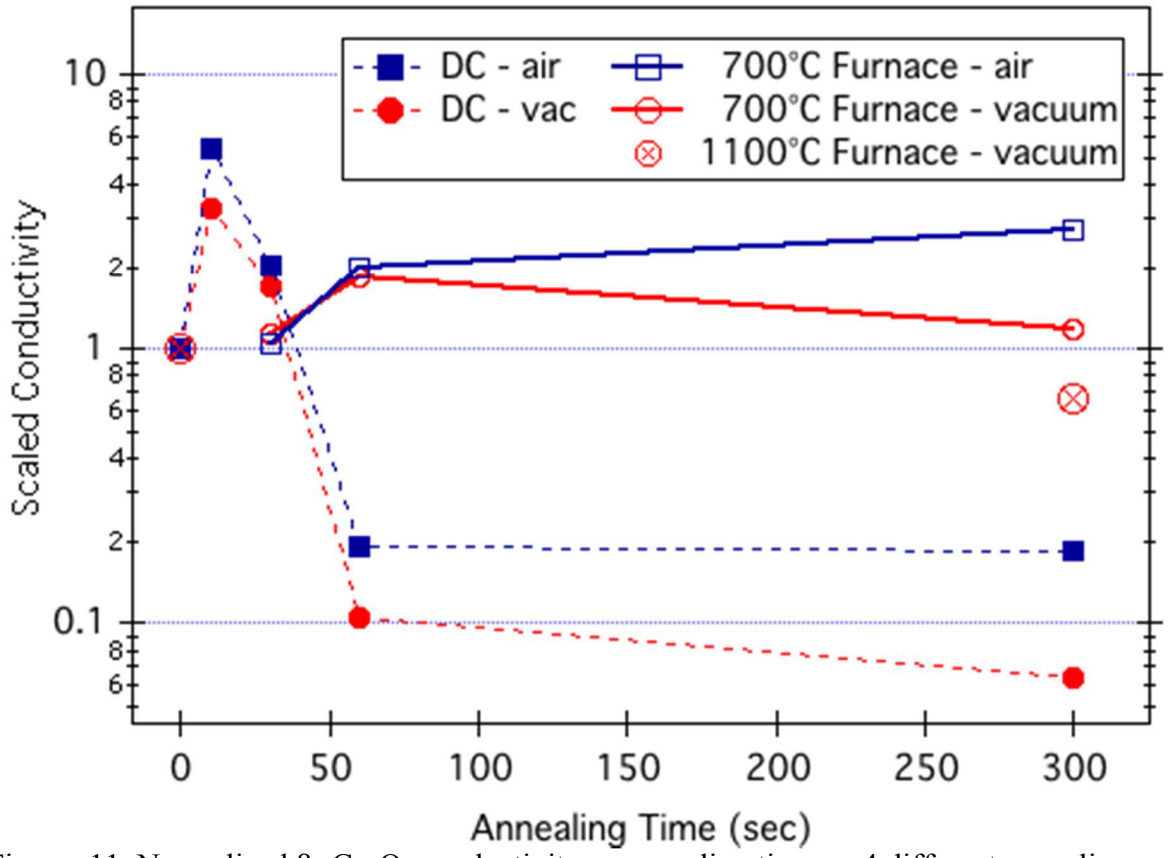

Firgure.11. Normalized β- Ga_2O_3 conductivity vs annealing time on 4 different annealing conditions.

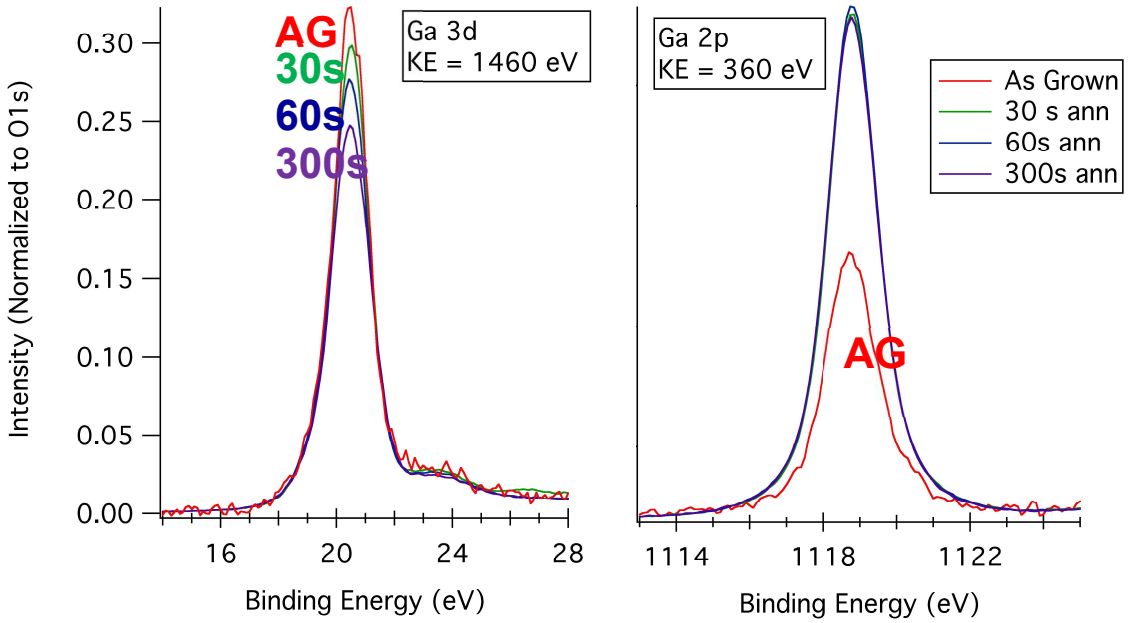

Fig.12 Single crystal XPS spectra after annealing

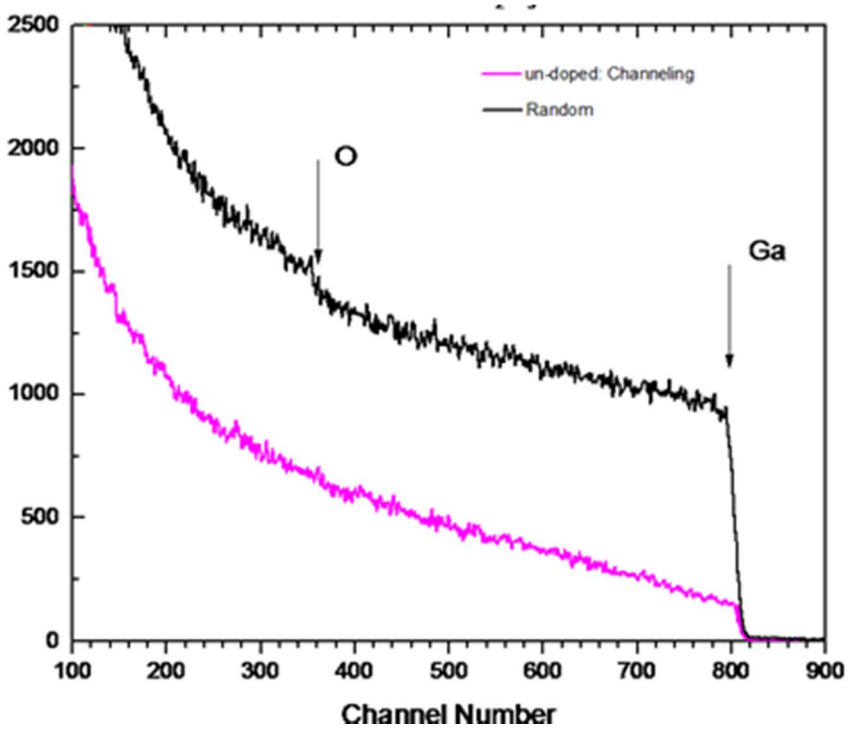

Fig.13 Rutherford Backscattering Spectroscopy on β- Ga_2O_3 at Channeling condition (Pink) and Random condition (Black)

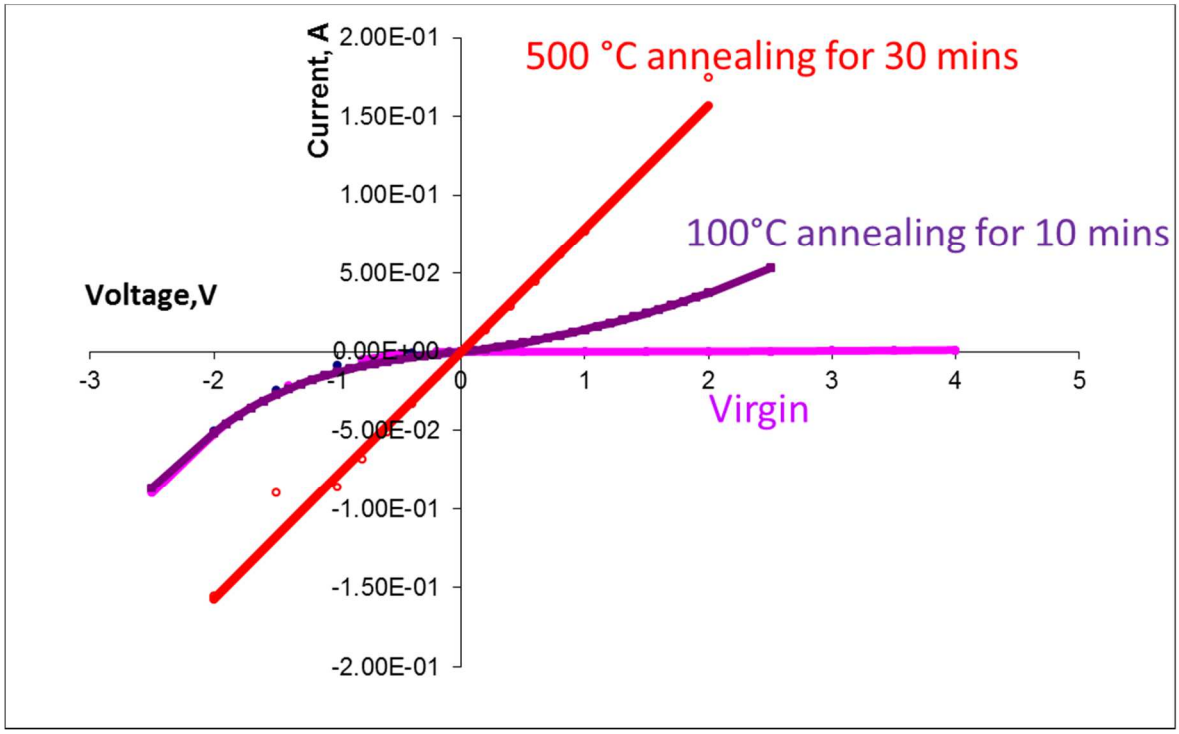

Fig.14 IV measurement of Ni/Single Crystal Ga_2O_3/Ti/Au structure before annealing(light purple), after 100ºC annealing for 10 mins(Dark Purple) and after 500 ºC annealing for 30 mins(Red), showing Schottky to Ohmic characteristics

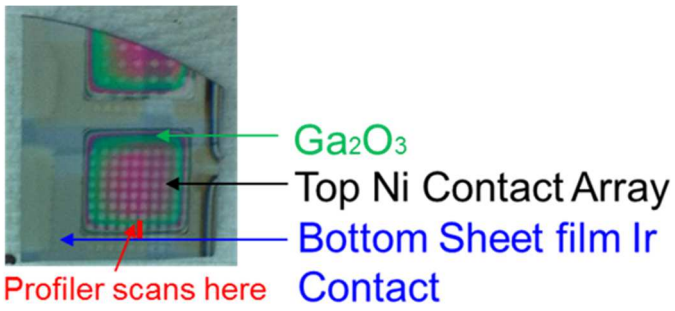

Fig.15 Top down view of Resistive switching device with Ni/Ga_2O_3/Ir Structure on Si Substrate

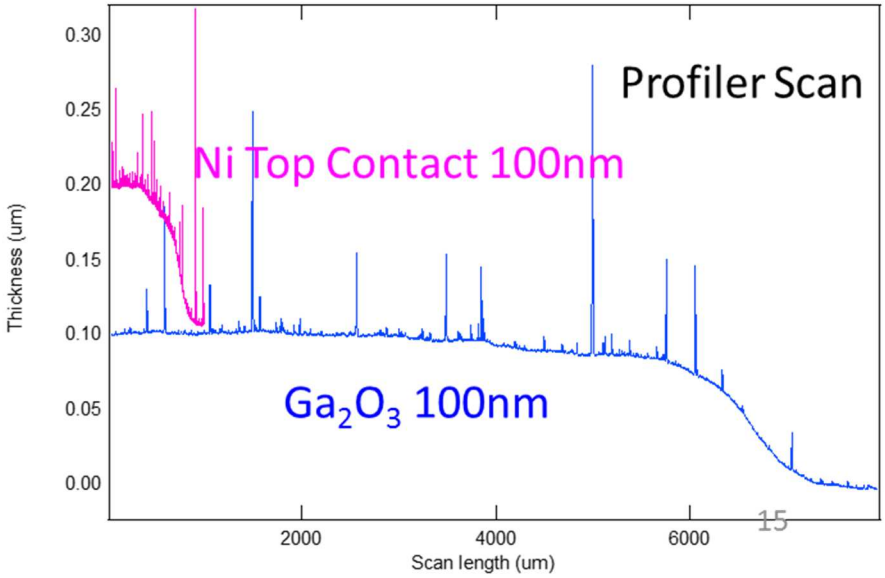

Fig.16 Contact and Film Thickness confirmation from Profiler

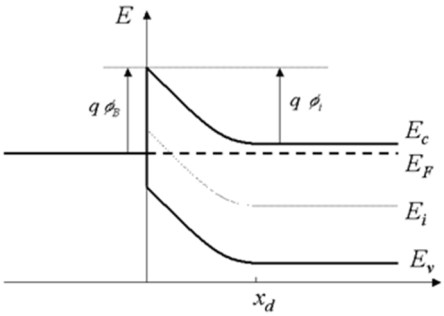

Fig.17 A standard schematics for metal to n-type semiconductor schottky contact

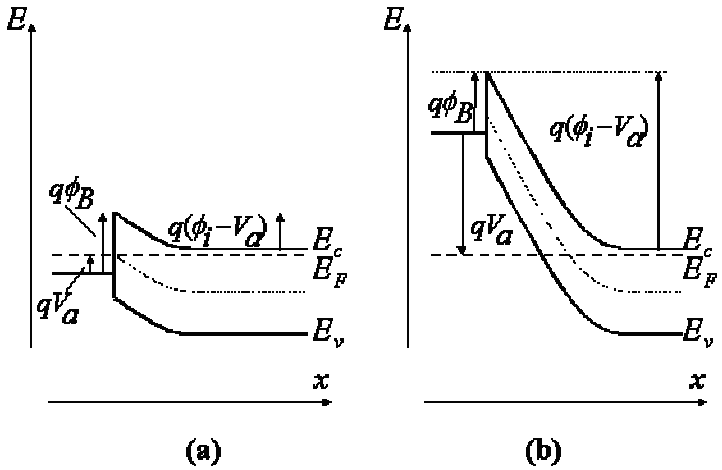

Fig.18 Barrier height change to a schottky contact after (a) subjected to a forward bias, (b) Subjected to a reverse bias

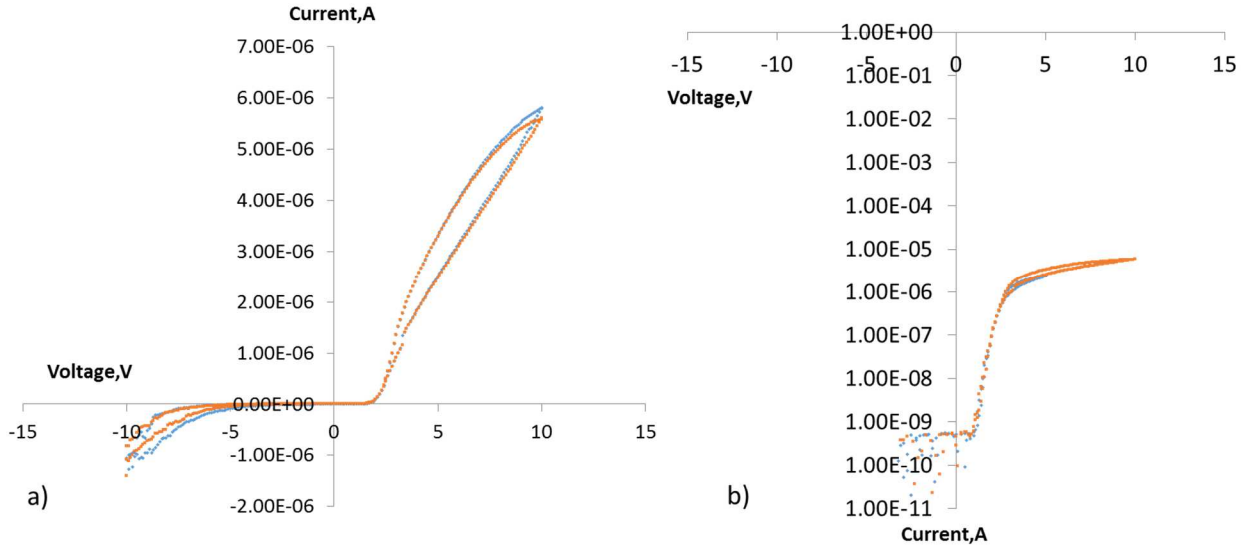

Fig 19 (a) Schottky hysteresis (b) Log scale of shottky hysteresis (1st repeat Red, 5th repeat Blue)

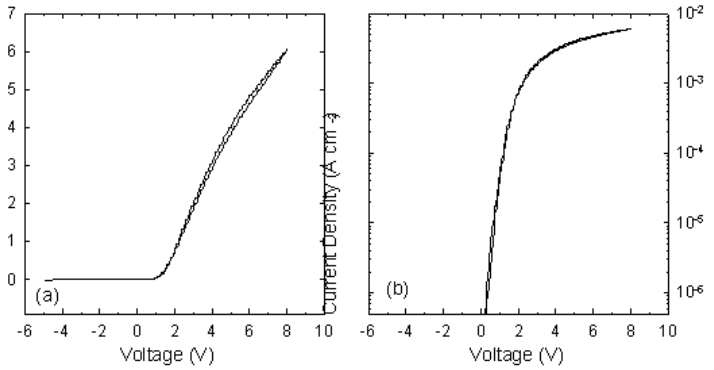

Fig.20 Common Hysteresis loop found in Pt/Si Shottky contact[4]

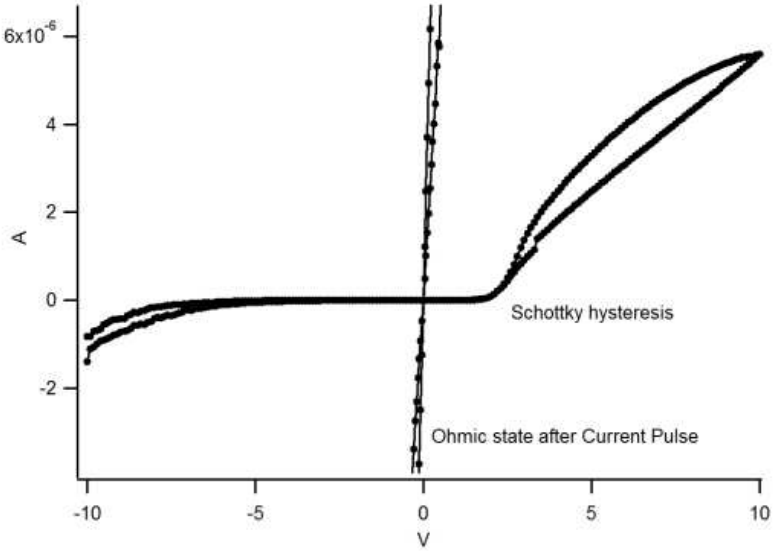

Fig.21. Comparison of IV curve of Virgin Sample before and after treated with 1 sec electric pulse

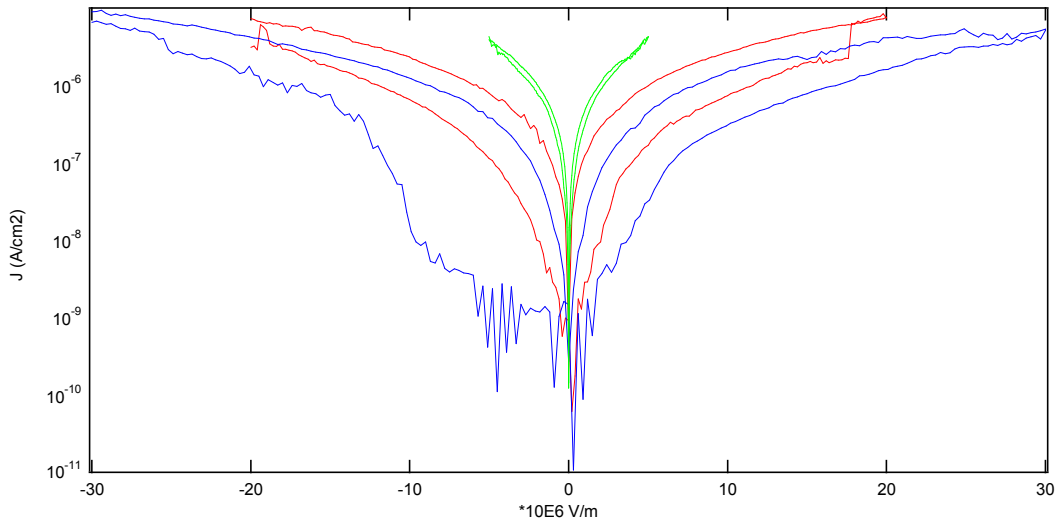

Fig.22. Current Flux vs electric field of pulse treated sample when switching under different electric field strengths

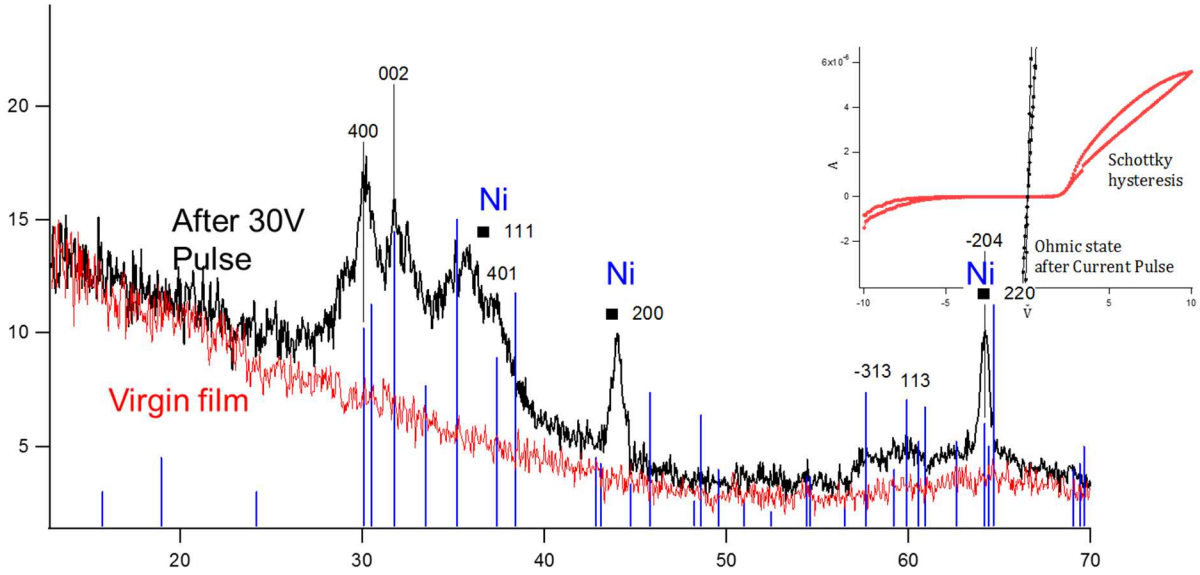

Fig.23. XRD before and after Pulse treatment

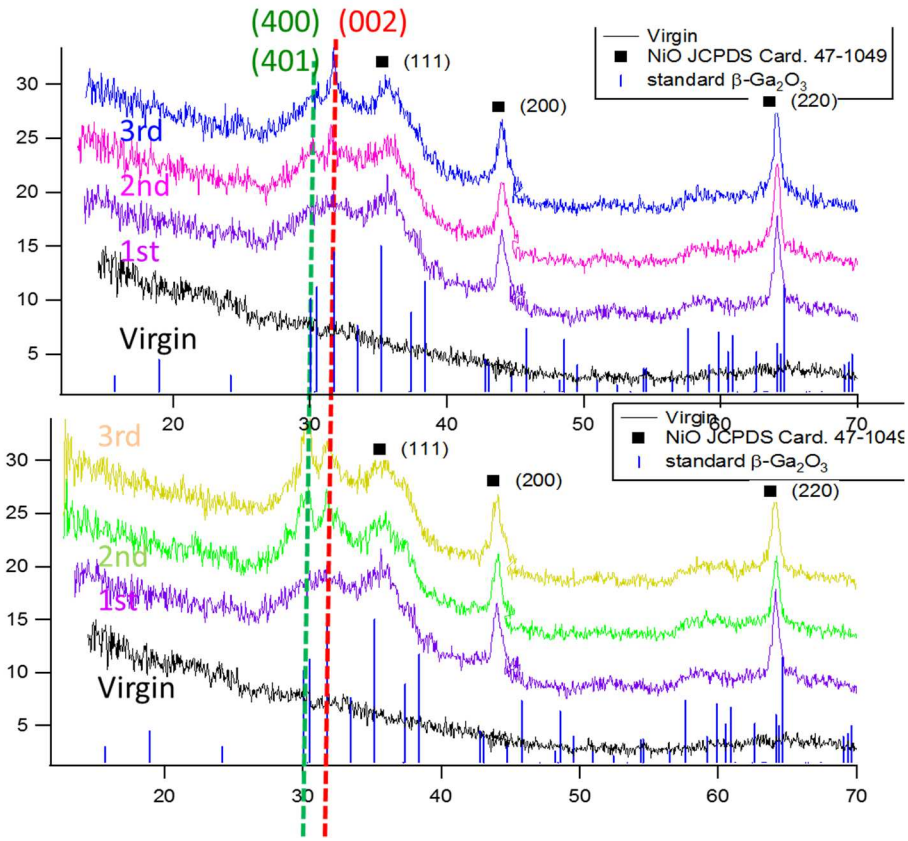

Fig. 24. XRD during resistive switching. Top: XRD post symmetric IV loop (Contact remains Ohmic). Bottom: XRD post asymmetric IV loop (When Contact changed between Schottky and Ohmic)

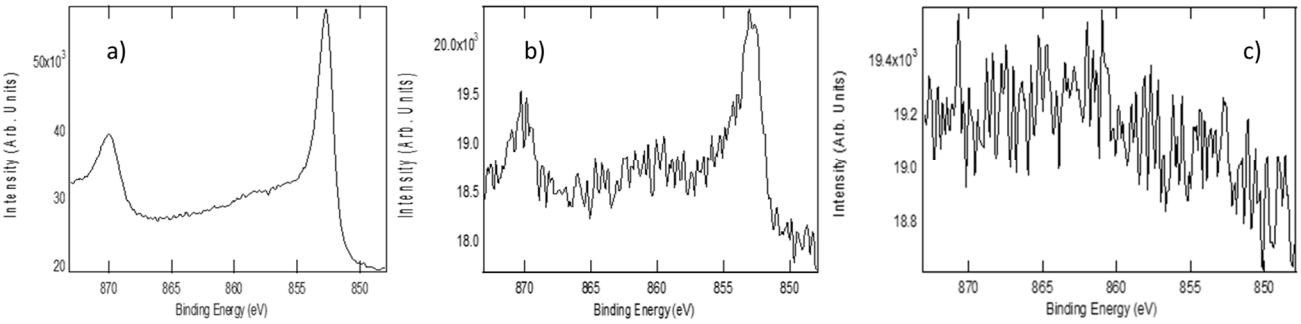

Fig.25. Virgin State: Ni3p Spectrum. a) Post 1 Sputter cycle b) Post 2 sputter cycles c) Post 3 sputter cycles

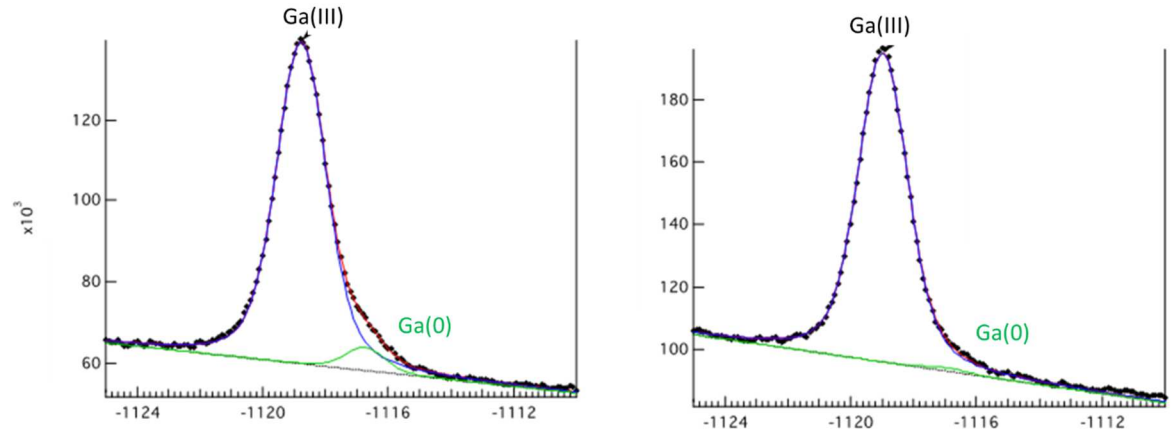

Fig.26. Virgin State: Ga2p Spectrum a) Post 1 cycle Sputtering. b) Post 2nd Sputtering

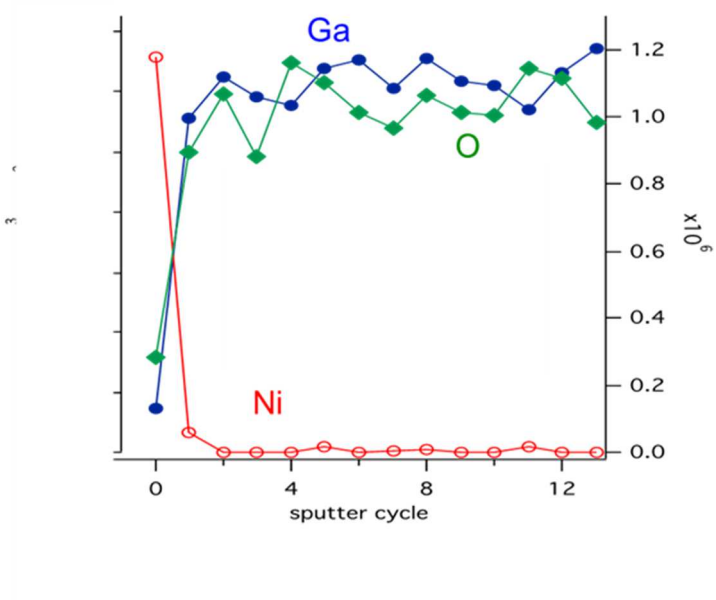

Fig.27. Virgin state : Ga and Ni Concentration profile from surface to depth based on area under the curve post each sputter cycle.

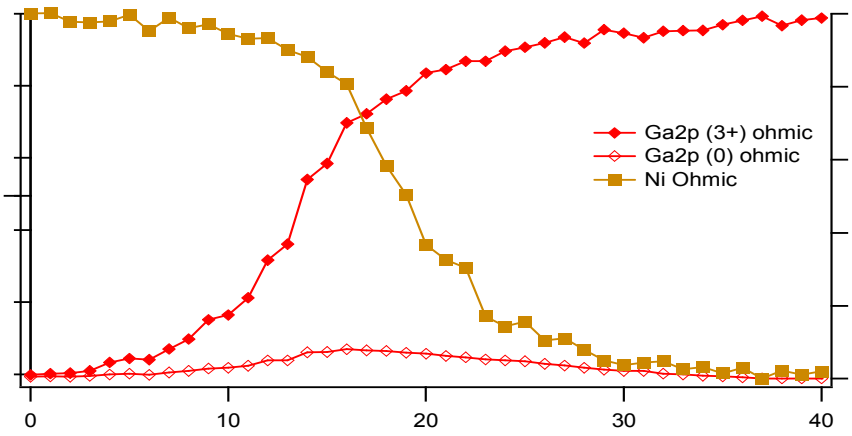

Fig 28. Ohmic State : Ga_{2p} (3+), Ga_{2p} (0) and Ni (0) signal vs sputter cycle

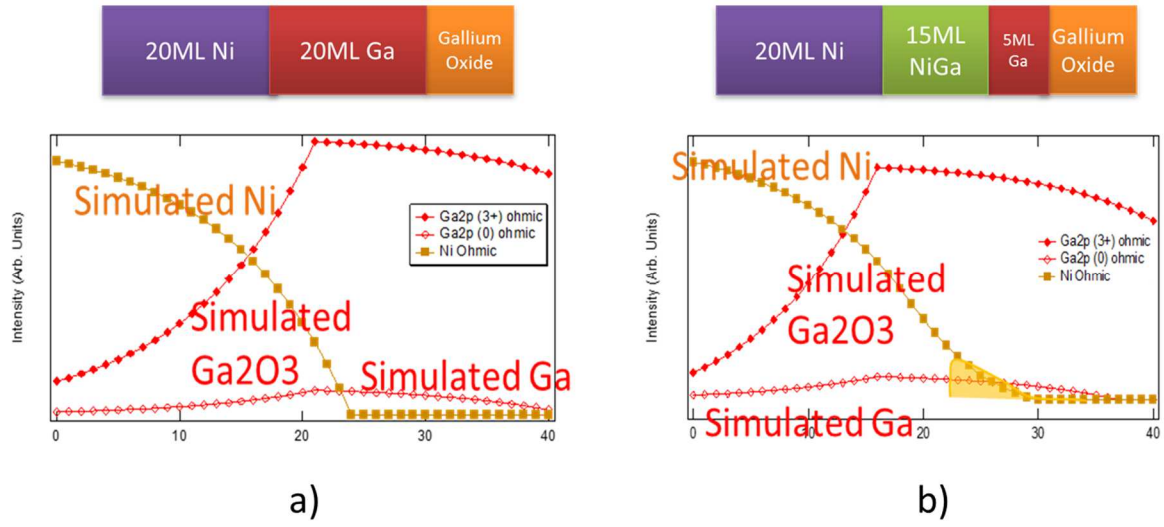

Fig 29. Ohmic State: Simulation based on Beer-Lambert Law, Case 1: 20ML of Ni, 20ML of Ga rich interface,(No Diffusion) Case 2: 20ML Ni, 15ML of Inter-diffusion zone, 5ML of Ga rich zone.(Diffusion). Case 2 fits better to actual profile (Fig.27)

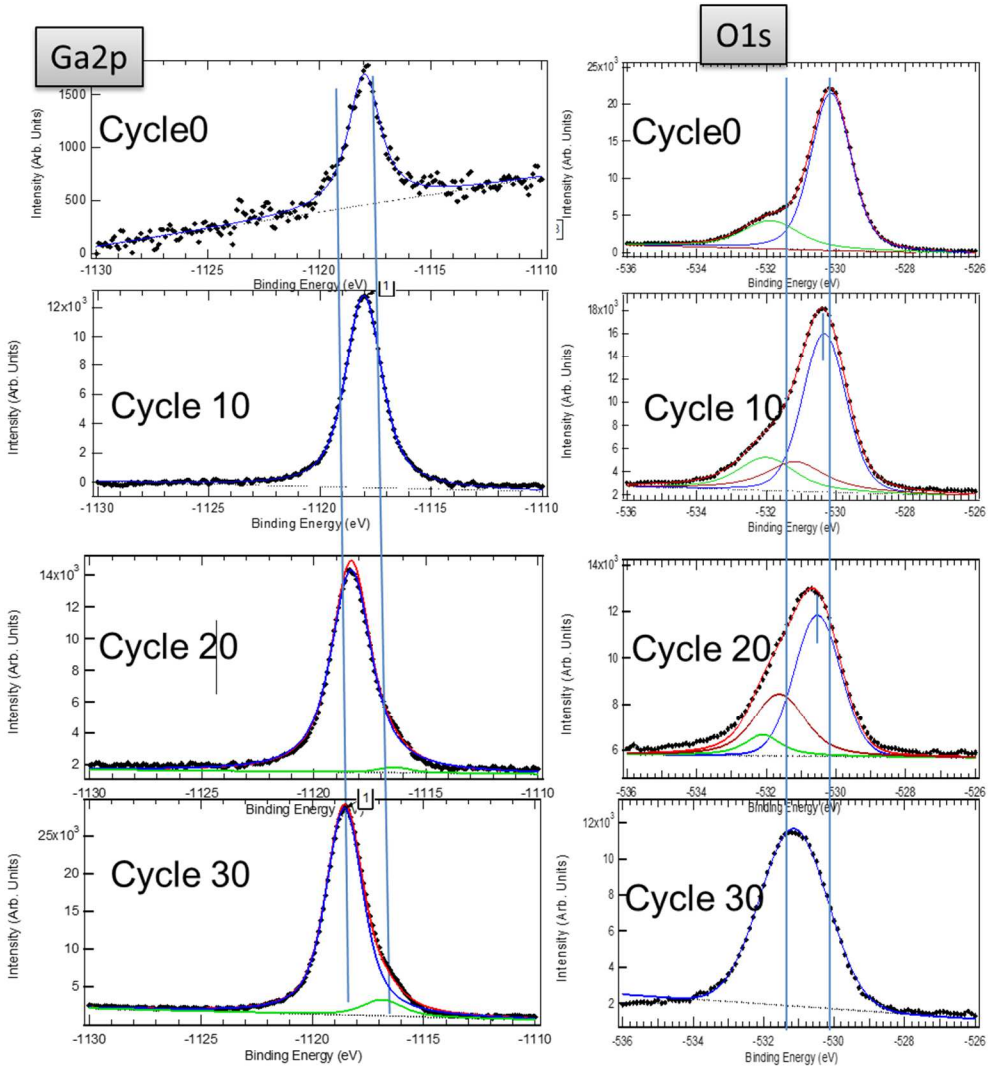

Fig.30. Schottky State: Evolution of Ga2p and O1s peaks over sputtering cycles.

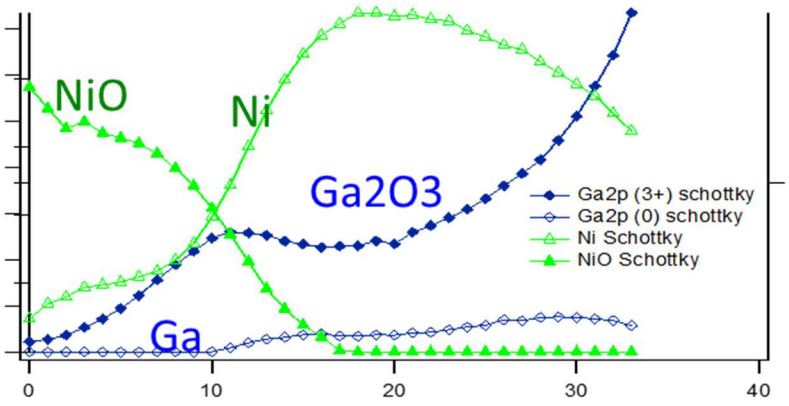

Fig.31. Schottky State: Ga2p and Ni3p signal over sputtering cycle.

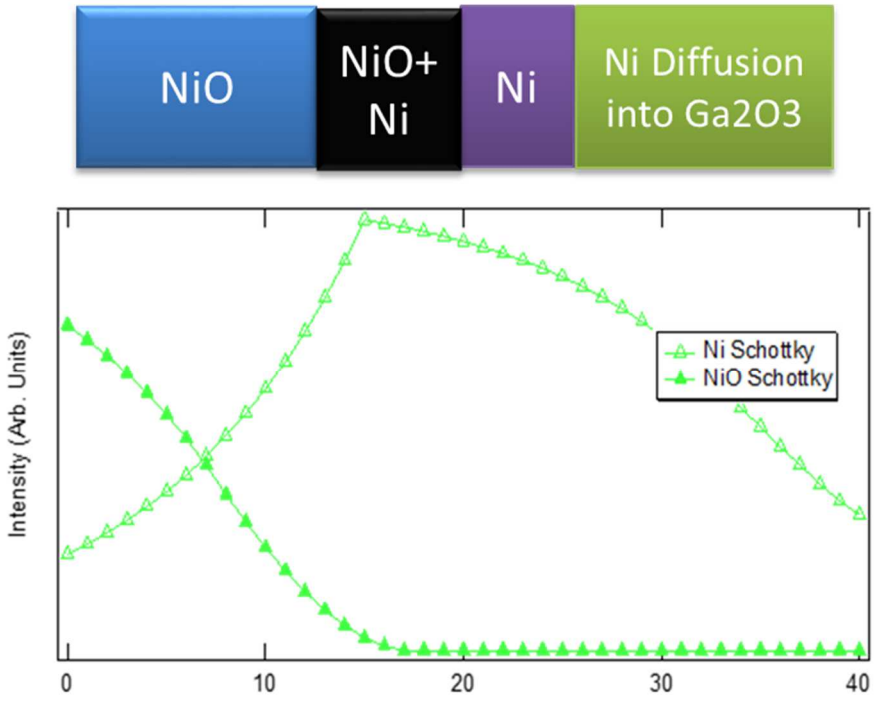

Fig.32. Schottky State: Simulation based on Beer-Lambert Law, 20ML of Ni being oxidized from surface, Ni/Ga2O3 interface is not oxidized.

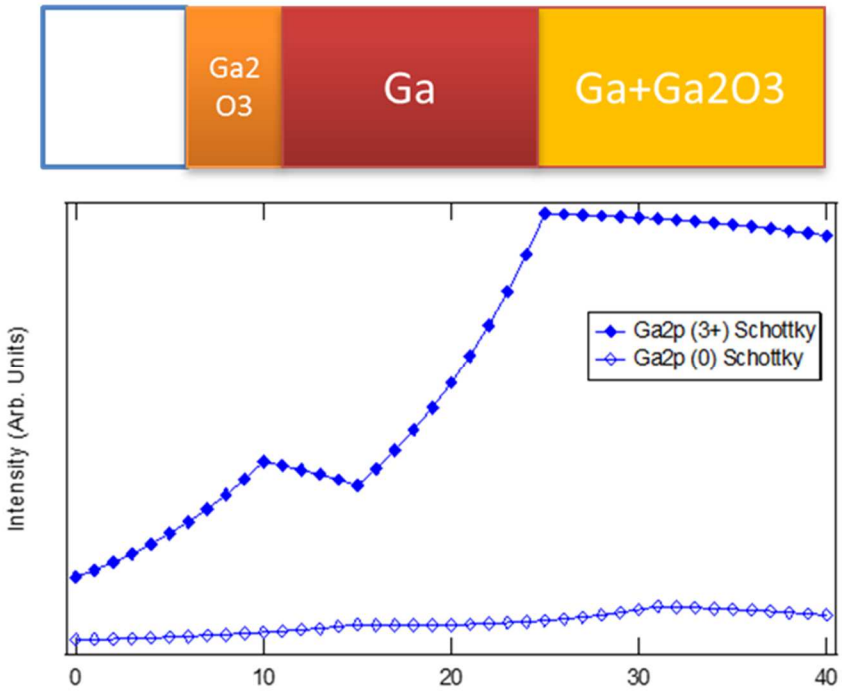

Fig.33. Schottky State: Simulation based on Beer-Lambert Law, Signal fingerprint from 10ML Ga2O3+10ML Ga+30ML Ga2O3.

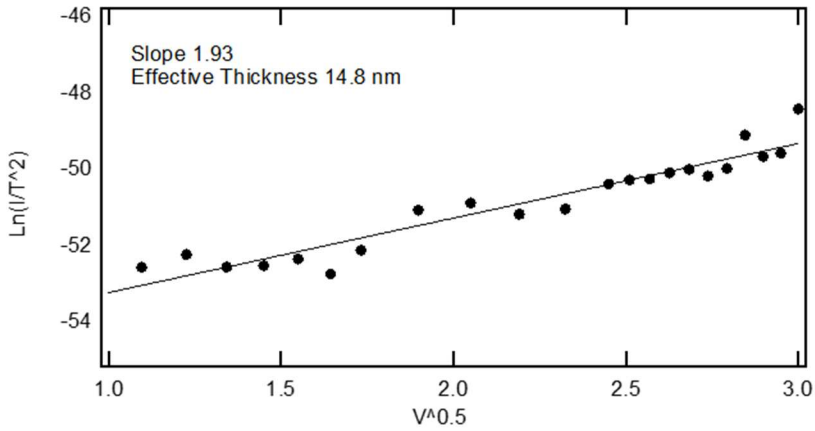

Fig.34. Schottky Emission slop for Schottky "off" state sample

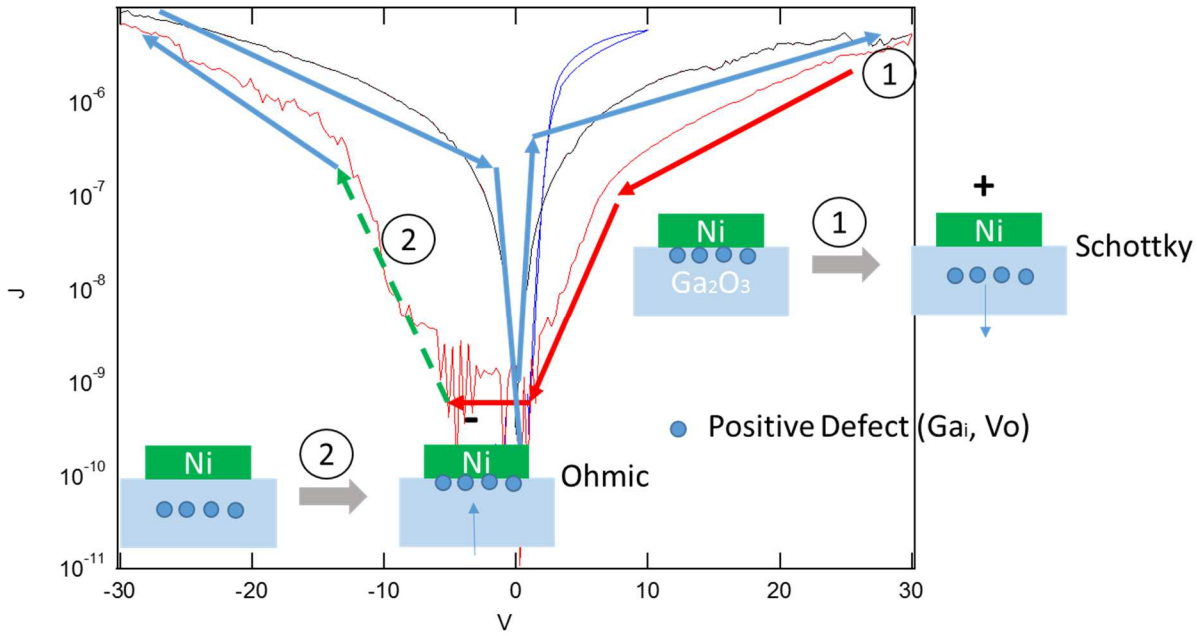

Fig.35. Summary of Schottky to Ohmic transition, where surface is bias differently. Positively charged defects are driven in and out of the interface, alternating the contact type

LIST OF TABLES

Sample ID	Atmosphere	Anneal temperature (C)	Annealing type	Duration of anneal time (s)
1	Ambient	Ambient	No	0
2	Vacuum	800	Direct Current	5
3	Vacuum	800	Direct Current	30
4	Vacuum	800	Direct Current	60
5	Vacuum	800	Direct Current	300
6	Air	800	Direct Current	5
7	Air	800	Direct Current	30
8	Air	800	Direct Current	60
9	Air	800	Direct Current	300
10	Vacuum	700	Furnace	30
11	Vacuum	700	Furnace	60
12	Vacuum	700	Furnace	300
13	Air	700	Furnace	30
14	Air	700	Furnace	60
15	Air	700	Furnace	300
16	Vacuum	1100	Furnace	300

No table of figures entries found.

Chapter 3.1.6

ACKNOWLEDGEMENTS

My sincere gratitude goes to my advisor Prof. Fumio Ohuchi, his patient guidance and immense knowledge not only turn myself from an ignorant young man to a successful engineer, but also helped me to go through the hardest period of my life over the past 3 years when I almost lost hope when dealing with life's turbulence.

Prof. Olmstead is another great mentor that I am lucky to work with. Her insightful opinions always provided me with refreshed ideas and brand new perspectives.

I am also thankful to Prof. Alex Jen. Prof. Marco Rolandi and Prof. Junlan Wang for serving as my committee members even at hardship.

Chapter 1. INTRODUCTION

1.1 REVIEW ON APPLICATIONS OF Ga_2O_3 AS WIDE BAND GAP OXIDE

Wide band gap oxides have wide usage in semiconductor industry. They can be good photo conductor, chemical sensor and transparent conductor, on the other hand, they are also good gate insulators, which appears to be contradictory to other applications. The key to their wide range of conductivity lies within their variety of conductivity mechanisms, and how they can be controlled and stabilized. Beta-Ga_2O_3 with a bandgap of 4.8 eV [5] and a highly anisotropic crystal structures, is well suited candidate for a study linking basic material science and device potentials.

Gallium oxide is widely known as "solar-blind" photo conductor, and its application in Ultraviolet signal detection under ambient conditions [6, 7]. Intrinsic Ga_2O_3 has high dielectric constant, which is utilized in III-IV based field effect transistor [8]. With Sn or Si dopant, it remains transparent in visible light spectrum, with electrical conductivity improvement, which opens its potential to be transparent conductive coating for solar cells [9], or transparent conductive substrates for GaN LED Growth[10]. When exposed to oxygen or reducing gas [8], its conductivity can be altered, which makes it a unique gas sensor [11, 12]. With injection of electron and holes, its electroluminescence application in Light emitting diodes has been explored. Its emission characteristic [13] spectra can be varied a lot, based on its intrinsic vacancy concentrations, rare-earth dopant types, and presence of impurities and foreign interstitials. First demonstration of Ga_2O_3 metal-oxide-semiconductor field effect transistors (MOSFETs) utilizes impurities such as Si and Sn as functional groups [14] while photoluminescence properties originated from incorporation of Eu3+ and $Tb_3Ga_5O_{12}$ into beta-Ga_2O_3 phase[15].

Despite its distinct potentials in multiple fields, it takes long time to implement proposed applications due to lack of understandings to conductivity mechanisms.

1.2 ORIGIN OF CONDUCTIVITY IN WIDE BAND GAP GA2O3

In the earlier studies, n-type conductivity in Ga_2O_3 is commonly attributed to oxygen vacancies. Oxygen vacancies are believed to act as shallow donors with ionization energy of 0.03–0.04 eV, based on inverse correlation between the conductivity and oxygen partial pressure during growth [16, 17] Meanwhile, report about Ga_2O_3 conductivity changes during annealing in oxygen environment [18] provided support to this model, claiming the conductivity changes was due to creation and removal of oxygen vacancies at surface. However as widely accepted dominant carriers, oxygen vacancies were not found as functional species in any reported FET application and device fabrication.

Most recent works done by Renyu Chen and Tracy Lovejoy in our group using Density Functional Theory with Generalized Gradient Approximation (DFT:GGA) [19], found that lowest activation energy of oxygen vacancies is 0.32eV, which makes it a deep donor instead of assumed shallow donor in oxygen vacancy model.

Varley[20] Also investigated the influence of oxygen vacancies and other impurities, and reached the same conclusion. Their calculation shows activation energies of oxygen vacancies are at least 1eV below conduction band minimum. On the other hand, Hydrogen interstitials, one of the defect that are commonly presented in materials treated in reducing atmospheres, was suggested to be an exclusive shallow donor in beta-Ga_2O_3 with transition level just above the CBM. Other than that, Si,Ge, Sn, F,and Cl are all possible shallow donor candidates if they are presented in Ga_2O_3 as dopants.

Although theoretical prediction has been made, the mechanism of conduction is still under debate. This is largely due to a wide variation in the quality of material fabricated by different synthesis techniques and the strong influence of processing history. As a result, it is difficult to combine literature results so as to reach a unified understanding of conduction in β-Ga_2O_3. Nevertheless, the following three models have been proposed for electrical conduction in β-Ga_2O_3.

While originally proposed oxygen vacancy model was proven flawed, impurities such as Hydrogen and Si are proposed as shallow donor band. Villora [21] experimentally demonstrated that impurities control electrical conduction in β-Ga2O3. In a double logarithmic plot of the electrical conductivity and Si impurity level (shown in Fig. 2), the conductivity continuously increased by over three orders of magnitude from a value as low as 0.03 Ω^{-1} cm^{-1} for 6N-purity crystals to 50 Ω^{-1} cm^{-1} for crystals with silicon.

2. It is also suggested that surface of pure beta-Ga_2O_3 has upward band bending by at least 0.5eV, the density of vacancies on the surface can be changed during varies treatment, causing the band bending to be suppressed, resulting in a reduction of contact barrier height [19].

Some key results have been obtained regarding the origins of conductivity in bulk β-Ga_2O_3, and some of the most complete studies have been conducted in the lab of our collaborator for bulk crystal growth. Electron spin resonance measurements [22] have shown that electrons in both intrinsic and Sn-doped samples are localized near the four-fold coordinated oxygen site, with equal populations overlapping tetrahedral and octahedral Ga [23]. Low-temperature conductivity measurements have revealed tunneling and hopping at low temperatures, followed by band activation above 100 K and carrier saturation above 220 K [21]. Variable conductivity has also been linked to variations in optical absorption and luminescence [24]. At room temperature and above, a mixture of ionic and electronic conductivity has been reported, with electronic

conductivity dominating above 900 K [25]. Above 1170 K, the conductivity scales with the oxygen partial pressure above the sample [12], a finding that is attributed to equilibrium between oxygen in the crystal and the ambient environment. The conductivity has also been found to be highly anisotropic (e.g., Fig. 6). However, the relative importance of anisotropy in the electron effective mass, carrier scattering, or the proximity of vacancy sites in a hopping conductivity model has not yet been elucidated. Theoretical predictions suggest V_{Ga}–Ga_i pairs dominate the intrinsic defects, with vacancy motion dominating conductivity under reduced conditions (2D or 3D) and interstitial diffusion dominating under balanced or oxygen-rich conditions (1D along channels).

1.3 BETA-GA_2O_3 AS A RESISTIVE SWITCHING MATERIAL

Whether conductivity in β-Ga_2O_3 is due to electron hopping/channeling, the existence of impurities as dopants, or dominated by surface defect concentrations which changes surface banding, all models and experimental results suggest several orders of magnitude change in the conductivity, indicating a possible insulator to conductor transition. A key question is whether we can precisely control the conductivity change at room temperature by altering the dominant type of defect concentration within the β-Ga2O3 lattice structure across a solid-solid interface, thereby making the change in conductivity reversible. Success in this regard will lead to the possibility of developing a new type of reversible resistive switching (RS) material

Resistive switching is the conductivity change of a Metal-Oxide-Metal system, which was due to the migration of metal cations or oxygen vacancies within oxide, during which a highly conductive state was formed. Despite various switching behaviors and materials are involved in the field, resistive switching can be generally categorized into two types of switching mechanisms by conduction mode in Low Resistance State (LRS), namely filament mode and interface barrier mode.

In filament mode, Current was injected through one metal contact, and flow through Oxide layer homogeneously and exits another contact. The conductivity is dictated by the bulk conductivity of the oxide, which is usually high to start with, therefore this state is referred to High Resistance State (HRS). After applying sufficient external stimulus, in most cases a large voltage across metal contacts, dielectric break down associated with formation of Metallic nano-bridges [26], oxygen vacancies (V^{2+}_O) composed conductive channels [27], dislocations [28] and so on are formed, creating a high conductive structure, which was usually with small cross-section connecting top and bottom contacts, named filament, which is always at higher conductivity state than bulk dielectrics. In this case, current flows through filament, resulting lower conductivity in the system. Further Joule heating will destroy the integrity of the filament, from metal re-oxidation, vacancy re-distribution and defect curing at evelated temperature in oxidizing environment, when the entire system is switched back to HRS.

In Interface barrier mode, Metal-Oxide-Metal system is intentionally engineered to be an associated with high contact barrier on one end, while the other side has low barrier height. The entire system starts with HRS, as electron needs to overcome high energy barrier at interface, when injecting from metal to oxide. External stimulus, i.e, large enough voltage, can drive defects, usually oxygen vacancies towards interface, which can reduce the barrier height of the interface and causes the system to be switched to LRS.

So far, a great variety of binary oxides have been reported with resistive switching characteristics, including NiO_x [29-32], TiO_2 [33, 34], and ZnO [26, 27, 35]. Among these binary oxides shares the same characteristics, which are listed below.

First of all, they all possessed abundance of defects, most commonly oxygen vacancies, and enough interstitial sites that allows the migration and agglomeration of defect.

Secondly, the formed low resistance state is relatively stable under room temperature even when exposure to oxygen environment. In NiO_x and TiO_2 system, the metal themselves exhibits multiple oxidation states. When oxygen vacancy accumulates to a certain level, cation can be reduced to a relatively lower valance state through redox reaction. In ZnO case, aggressive switching may lead to Zn formation during electrochemical induced redox reaction. In either case, formation of LRS is achievable at the presence of electric field, and preserved when field is removed.

Thirdly, system can be subjected to curing process to re-distribute agglomerated vacancies, or get back to HRS through self-oxidation with heat.

Whether Ga_2O_3 can be a good candidate for RS material, lies within its structural studies.

Chapter 2. MATERIAL BACKGROUND

2.1 MATERIAL STRUCTURE REVIEW

There are five phases (α, β, γ, δ, and ε) of Ga_2O_3, in which β-Ga_2O_3 is the only stable modification at high temperature that remains stable upon cooling.[36] The crystal structure of β-Ga_2O_3, shown in Fig. 1 (reproduced from [1]), is a base-centered monoclinic with lattice parameters a=12.23 Å, b=3.04 Å, c=5.80 Å and =103.7° (between a and c). There are four Ga_2O_3 units per crystallographic unit cell (which comprises two primitive unit cells), each with two inequivalent Ga sites and three inequivalent O sites. Half the Ga atoms are in Ga(I) sites, which form slightly distorted tetrahedra with four O ions, and the other half are in Ga(II) sites, which form highly distorted octahedra with six O ions. Each O(I) is threefold coordinated and lies at the intersection of two octahedra and one

tetrahedron. Each O(II) is also threefold coordinated and is shared between one octahedron and two tetrahedral, while each O(III) is fourfold coordinated and lies at the corner of three octahedra and one tetrahedron. These octahedra and tetrahedra are aligned along the b direction, leading to the formation of 1D channels. A layered structure is observed on the [100] planes, in which two types of surface terminations may exist. “A termination,” which consists of all oxygen terminated planes, is formed after cleaving Ga(II)–O(II) bonds, whereas “B termination” is the cut-off plane at nearest-neighbor rows of Ga(II) and O(III) atoms, each singly-unsaturated. Ga(I) and O(I) atoms at the surface are fully coordinated, and there are no O(II) atoms in the surface plane. Consequently, a plane consisting of both Ga and O is formed.

2.2 DEFECTS IN BETA-GA_2O_3

Point defects play a major role in electrical conduction. In general, there are several different types of point defects that can be formed in a crystal.

1. Vacancies: Unoccupied sites that are usually occupied by an atom.
2. Interstitials: Atomic sites that are usually not occupied by atoms and are thus in high energy configurations. Only small atoms can occupy interstices.
3. Frenkel defect or Frenkel pair: A nearby vacancy and interstitial pair. This is created when an ion moves into an interstitial site, thereby creating a vacancy.
4. Schottky defect: A pair of vacancies in an ionic solid.
5. Substitutional defect: An impurity or dopant that is incorporated at a regular atomic site in the crystal structure.

Tracy Lovejoy's work [19] suggested that the lowest formation energy of O vacancies is 0.71eV at neutral O(II) site, while lowest formation energy of Ga vacancy is 0.28-0.49eV in neutral tetrahedral site and octahedral site, or 0.72eV in negatively charged octahedral sites, suggesting Gallium Interstitial-Vacancy pair is more preferential in the lattice.

Chapter 3. SINGLE CRYSTAL GA2O3 STUDY

As introduced, the first goal of my research is to elucidate connections between defects and conductivity in beta-Ga_2O_3.

3.1 SINGLE CRYSTAL CHARACTERIZATION

A direct investigation of the contributions of defects in Ga_2O_3 requires an initial sample with almost no defects, preferably a single domain specimen with no uncertain contribution from grain boundaries, crystal orientation, or defects that are readily incorporated before treatment.

However, a direct approach is very difficult to implement due to several obstacles that are encountered.

Firstly, Ga_2O_3 Single crystal is hard to obtain, no commercial product was available until 2015, and only limited number of lab in the world can fabricate high purity single crystals.

Secondly, intrinsic Ga_2O_3 is electrically insulating with high surface charging, which renders most metal-Ga_2O_3 contact non-ohmic. This in turn makes direct electrical measurements of the conductivity harder to be interpreted, as it is difficult to separate bulk and interface effects.

In addition, the high resistivity or up-ward band bending and abundance of surface charges in Ga2O3 hinder the ability to obtain clear and reliable signals from most electron-based microscopy

techniques, which makes direct observations of vacancy site formation and migration during treatment difficult.

Thirdly, even with close to ohmic contact applied to the crystal, high-temperature treatments can easily damage the contact quality due to surface oxidation and contact diffusion. This not only changes the contact barrier height, but also reconfigures the contact geometry. Consequently, electrical measurements obtained before and after annealing can vary due to only contact modifications not material property changes.

In the following paragraphs, the method used to fabricate a single domain crystal is outlined and a new approach to conducting direct current measurements of Ga_2O_3 is proposed and carried out with the goal of performing more reliable and accurate electrical research on Ga_2O_3.

3.1.1 *Single crystal fabrication*

The first of the aforementioned obstacles can be resolved by growing single crystal β-Ga_2O_3 with the lowest possible concentration of defects for use as the starting material.

β-Ga_2O_3 single crystals were grown at the National Institute for Materials Science using a floating zone (FZ) technique with four halogen lamps and corresponding ellipsoidal mirrors. Briefly, a feed rod was prepared using 4N purity Ga_2O_3Ga2O3 powders and subsequently cold pressed and annealed in air at 1450 °C for 10 h. A single crystal was grown with a pulling down rate that varied between 1 and 5 mm/h and a constant gas flow rate of 250 ml/min in an O_2 and/or $_{N2}$ environment. Single crystals with different orientations were used as seeds in order to fix the growth orientation and examine the stability of the growth process. Our crystals were grown in the <100> direction with a [001] cleavage plane. The purity of the crystals was 99.99%, with the main impurity being Si. Shown in Fig. 3 is a sample rod that was used in my research.

3.1.2 *Contact*

In order to carry out direct current measurements, an investigation of various protocols to achieve reliable ohmic contacts was performed. It was confirmed that both Ti/Au and Ir evaporation on Ga_2O_3 single crystals can produce ohmic contact. The electrical measurement contact was prepared by thermal evaporation of a Ti interlayer, followed by Au evaporation in a vacuum chamber at 10-8 Torr base pressure so as to minimize excessive oxidation of Ti interlayers. Typical thicknesses of the Ti and Au layer were 100 and 3000 Å, respectively. Further contact was made using Ag paste followed by the attachment of Cu wires. Transport and surface measurements were subsequently obtained.

As mentioned above, even when good ohmic contact is initially established, contact oxidation and diffusion at elevated temperature still create obstacles to high-temperature measurement. Initial experiments have 4 Spot Ir contacts deposited along <010> direction on [001] surface of the crystal before annealing, however, surface composition analysis shows Ir migrated several millimeters across the sample surface post anneal. Therefore, mechanically (i.e. pressing the crystal against Ta Foil) applying non-ohmic, non-diffusive Ta contacts to the sample prior to heating can prevent the contact material front from diffusing throughout the surface of the sample during effective direct current annealing. For annealed samples, ohmic contacts were deposited after annealing for further analysis.

3.1.3 *Experimental procedure and data analysis*

Thin slices of Ga_2O_3 single crystalline samples were cleaved to expose a (100) plane in air, which is the cleavage plane as the result of layered structure of monoclinic phase, and channeled structure

along <010> (b) direction. Although the material used in the present experiment was at its best possible purity, there is a slight variation in the crystal quality at different locations in the bulk crystal. To be consistent for all measurements, all samples were prepared in the following way; A piece of 15mm-length (in c-direction) x10mm-width (in b-direction) x 0.1mm-thickness (in a-direction) was extracted from the middle section of the bulk single crystal rod, where the crystal quality was assumed to be uniform. This piece was further cleaved parallel to the b-direction into 5 smaller pieces with a dimension of ~3mm (in a direction) x 10mm (in b direction) x 0.1 mm-thickness (in c-direction). In this way, each experiment can use up to five samples which are similar in terms of crystal qualities and dimensions.

3.1.4 *PPMS*

Our preliminary studies has shown that, pure Ga2O3 Ga_2O_3 [3] displayed a strong variation in conductivity during standard UHV surface preparation that likely arose from a combination of bulk and contact effects. As-cleaved samples were highly resistive (> 50 MΩ across long dimension of 1 x 4 x 12 mm sample); application of a voltage pulse (~200-400 V, ~1 s) drawing less than 0.1 A switched the samples into the 102-103 Ω range. Prolonged heating around 800-1000 °C in UHV (20-200 min) to obtain good surface order for LEED and STM caused the resistance to rise to 104-105 Ω or higher, after which further heating could only be achieved by another voltage pulse to return the sample to a relatively conductive state. As many as ten such cycles were observed with some samples before sample degradation caused a visible break in the sample with darkened regions extending a few mm. X-ray diffraction revealed many crystalline grains with random orientation near the break, and very few or only one grain (single crystal) far

from the break. No jumps in resistance were observed upon cooling. Crystals Intentionally doped with Si displayed good conductivity with no switching characteristics, perhaps because a large local field is never built up, but show similar polycrystalline breakdown after prolonged heating. With these preliminary measurements, I conducted systematic measurements of the electrical conduction of β-Ga_2O_3.

For a conventional doped semiconductor, such as n-Si, temperature dependence of the carrier concentration can be seen in Fig. 4. At very low temperatures (i.e., large 1/T), the donor electrons are bound to the donor atoms and thus, the transport properties can be investigated without considering the direct excitation of donor electrons into the conduction band. As the temperature is raised, ionization of donor electrons becomes dominant, and at temperatures above 100 K, all of the donor electrons are ionized, at which point the carrier concentration is determined by doping levels. The region is called the extrinsic (or saturation) region. In this region, an increase in temperature produces no increase in carrier concentration. At high temperatures, the thermally generated intrinsic carriers outnumber the dopants in the intrinsic region, where the carrier concentration increases exponentially with temperature.

3.1.5 *Scanning Tunneling Microscope (STM)*

Decreased conductivity after direct current annealing under high vacuum, together with increased dimensionality of hoppings suggest that oxygen vacancies are not the primary contributor to conductivity. If vacancies are created during annealing, we would expect to see them accumulate on the surface, as they are introduced through vacuum-Crystal interface. A scanning tunneling

microscope (STM), an instrument analyzing samples surface at atomic scale with 0.01nm depth resolution, is chosen as our technique in identifying surface reconfiguration during annealing.

A sample with 3mm (in c direction) x 10mm (in b direction) x 0.1 mm-thickness (in a-direction) in dimensions was mounted on STM sample holder, with 2 ends along b direction clamped with Ta clips. One side of the clip is grounded while the other one applied to a Agilent voltage source, allowing a ~10V voltage to be applied to the sample under 10^{-10} torr vacuum prior to STM scans. Sample temperature was adjusted to 800 ºC and recorded using optical pyrometer.

The sample is subjected to different length of direct current treatment, namely 4 sec, 17 sec, 45 sec, 180 sec, 7200 sec and 20 hours. After each treatment, a STM scan is taken in order to probe gradual evolvement of surface structures.

3.1.6 *Conductivity vs. Annealing time*

STM scans give a direct indication that surface structure progressively changed during annealing, so to do the electrical analysis with sample 'before annealing" and "after annealing" is too simplified and generalized. For a better understanding of the conduction mechanism, electrical measurements at each stage of the annealing process should be performed so that a direct relation between surface configurations with conductivity can be established.

As described in table 3.1, different samples with identical crystal quality and dimensions were prepared, and 4 of the samples were subjected to 10^{-8} Torr direct current non-ohmic contact annealing for 5 sec, 30 sec, 60sec and 300 sec. After that, non-ohmic contacts were removed followed by Ti/Au electrical contact deposition. Resistances were measured by 4-point probe method, and conductivity were calculated based on the sample geometries.

For better comparison of how vacuum, oxygen or H2 atmosphere influence the conductivity change with respect to annealing time, another 2 sets of experiments were done by annealing in Air and in 5%H_2/95%Ar.

3.1.7 *X-Ray Photoemission Spectroscopy (XPS)*

The surface morphology change observed in Scanning Tunneling Microscopy, and defect migration/disordering proposed by variable range hopping analysis, can be supported by the surface electronic structures and chemical composition change using X-ray photoelectron spectroscopy (XPS) technique, which is a surface-sensitive quantitative technique that measures the elemental composition and electronic state of the elements.

XPS spectra are obtained by irradiating a material with a beam of X-rays while simultaneously measuring the kinetic energy (KE) and number of electrons that escape the material being analyzed. Because the energy of a particular X-ray wavelength is known, the electron binding energy (BE) of each of the emitted electrons can be determined by using an equation below

Where Ephonon, Ekinetic and Φ are incident X-ray energy, kinetic energy of photoemission electrons, and work function of the spectrometer, respectively.

Based on the formula above, with the fixed phonon energy and work function, electrons with lower binding energy have higher kinetic energy after photoemission. Kinetic energy of the electrons is positively related with the electron mean free paths as shown in Fig.5 above 50eV, so higher mean free path can be achieved with analyzing electrons of lower binding energies. On the other hand, increasing incident phonon energy can also increase the kinetic energy and mean free path of photoelectrons.

The escape depth of the electron is proportional to the mean free path; it is also related to the detector position. It increases with increasing detector angle to the sample surface at which the photoemission occurs, and eventually reaches maximum when the detector is normal to the surface plane.

By combining control of electron mean free path and analysis geometry, a non-destructive depth profile analysis can be achieved, allowing us to investigate the defect migration by looking at the dependence of composition and depth.

Our PHI XPS system in University of Washington has Al Kα X-ray source with the phonon energy of 1.486kV with maximum analyzing depth about 3-5 nm. The relative angle between detector and sample stage can be changed from 10-90 degree, which makes the grazing angle analysis on the top several atomic layers possible.

Ga3d was chosen as bulk information peak since its KE=1460eV with mono-chromatized Al Kα X-ray source. All Ga_{3d} peaks were taken with analyzer at 75° to further increase the probe depth, in order to get bulk information. On the other hand, Ga_{2p} with KE of 360 eV was taken at 30° for more surface sensitive analysis. All data were normalized to O1s peak taken at 75° and 30° respectively.

Similar setup as in STM was used in XPS system, which a piece Ga_2O_3 was clamped with Ta foils for non-ohmic contacts, and in-situ treated with DC before each scans at about 500-degree C. However due to equipment limitation, the base pressure was 10^{-7} Torr, which was higher than STM study.

3.1.8 *Probe of Interstitial Atoms by Rutherford Backscattering Channeling*

Another approach to investigate the existence of interstitials is through Rutherford backscattering spectrometry. By irradiating a high energy incident beam on the sample, the elastic collision between particle from the incident beam and a stationary particle located in the sample can be occurred. By comparing a complete channeling position showing least back scattered beam energy, with a random position showing strongest yield on back scattering, a χmin value was obtained, suggesting the crystal quality of the sample.

The Rutherford Backscattering measurements on β-Ga_2O_3 sample and are along <100> axial directions using 2.0 MeV He^+ beams accelerated by a 3.4 MV tandem accelerator. The χmin value is estimated by the backscattering yield ratio at high energy (channel number 800), which is corresponding to the scattering from Ga in the crystal.

3.2 Data Analysis and Discussion

3.2.1 *High temperature vs Low temperature Conductivity in PPMS*

It is my objective to elucidate how the defects can contribute to the electrical conductivity. To assess this question, I do not want to create a situation where carriers thermally excited across the band gap, exhibiting the roles of defects in electrical conduction; for this reason, I have purposely investigated the electrical conductivity at low temperature (below RT) in details. Shown in Fig. 6 is electrical conductivity σ of "as-grown" and "vacuum annealed" β-Ga_2O_3 parallel and perpendicular to the open-channel b-direction. Below room temperature, multiple temperature regions with different functional dependence σ(T) were observed with somewhat different

transitions between these regions depending on current direction and thermal processing. The anisotropy decreased after vacuum annealing, and the functional dependence also changed. Below, I discuss fitting of $\sigma_b(T)$ (b = parallel to the one-dimensional channels) to various transport models; in particular, a change from one-dimensional to three-dimensional variable-range hopping with annealing was found, which might indicate increased disorder along the channels after annealing.

Temperature above 50 K (but not exceeding RT): In this temperature region, the conductivity data were plotted in Fig 7 with respect to temperature in log(σ) versus 1/T form (i.e. an Arrhenius form), since the donor electrons follow the direct band conduction as:

Where k is Boltzmann constant, T is temperature and Eg is the activation energy, or the energy band difference between donor band and bottom of the conduction band. With appropriate slop fitting, the activation energies for "as grown" and "as annealed" samples were found 32 meV and 20 meV, respectively. This activation energy indicates a shallow donor – consistent with silicon impurities in a low dielectric constant material – which is more than an order of magnitude less than that predicted for oxygen vacancies. Change in the activation energy values before and after annealing might be attributed to the variation of crystal structure, since three order magnitude changes in the conductivity are likely due to both changes in the carrier concentration (n) and mobility (μ) terms in $\sigma=en\mu$. Here, the mobility is proportional to the carrier mean free path and thus, any change in the defect concentration by the lattice distortion can decrease the mean free path of electrons.

Temperature below 50 K: In this temperature regime, the thermal energy is below 4 meV and thus, the thermally activated process of carrier conduction is minimized. Instead, electron hopping and channeling can be responsible for the conductivity. The channeling path can be either vacancies, or interstitials. Mott's conduction model suggests that the degree of carrier hopping in one, two or three dimensions, can be determined by properly fitting the conductivity data with modified temperature in a form described below.

In this equation, one dimensional (1-D) hopping suggests a hopping path along the chain with a uniform distribution of delocalized states, while two (2-D) and three (3-D) dimensional hopping can suggest a less uniform distribution of hopping sites and inter-chain coupling.

Shown below in Fig 8 are attempts to fit the ln(σ) data with respect to $T^{-1/2}$ (or $T^{-1/(1+1)}$) for 1-D, $T^{-1/3}$ (or $T^{-1/(2+1)}$) for 2-D and $T^{-1/4}$ (or $T^{-1/(3+1)}$) for 3-D. It was found that the ln(σ) data for "as grown" sample was fit well to a $T^{-1/2}$ model, whereas that the ln(σ) data for "as annealed" sample was fit well to a $T^{-1/4}$ model. To correlated with the data, "as grown sample" shows variable range hopping in one dimension (1-D) along b direction, while "annealed" results suggest three dimensional hopping (3-D) based on Mott's Law.[37, 38] There are two possibilities that explain the cause of hopping mechanism changes. When the delocalized states are formed by defects in interstitial sites, the aligned defect is a 1-D conduction path for which constrains electron hopping well within the channel, while hopping mode changes to 3-D when defect change is disrupted by in-plane and out of plane thermal migration. On the other hand, when electrons are traveled in other delocalized states, defects are acting as scattering site along channeled direction. Aligned defect reduces the scattering of electrons along channel direction. On the other hand, introduction of oxygen vacancies and/or Ga interstitials into channel structure creates more scattering centers.

In either case, the directional constrains of VRH in unannealed sample suggests single dimensionally aligned defects, which also attributes to highly anisotropy conductivity. This defect chain is preserved after single crystal growth and sample preparation, but with long annealing, defect alignment is gradually disrupted by inplane and out-of-plane thermal migration.

This structural variation with annealing may be monitored by Scanning Tunneling Microscopy (STM), which will be described next.

3.2.2 *Surface evolution from during annealing*

Meaningful interpretation of the STM data, however, requires knowledge about the surface structure. In the previous publication [3] we experimentally determined that the primary beta-Ga_2O_3 (100) surface termination was an atomic plane consisting of gallium and oxygen (called "B" termination) with the "A" termination (oxygen only) present only in small amounts at step edges. The step height was exactly one-half of the unit cell distance (0.56nm). Preferential termination at either A or B was the likely cause of the uniform step height when viewed in a large scale. At a smaller scale, however, we observed additional very small terraces consisting of A termination. Larger B terminated terraces were consistent with the theoretical result that the B termination was the more energetically favorable.

We present in Figure 9 a series of STM micrographs after in-situ annealing with time at 800 °C. It is found that overall change of the surface occurs from large uniform terraces to introduction of holes consistent with random removal of half a unit cell (to the next "B" surface layer). With

prolonged annealing, up to five terrace levels were exposed in a 100x100 nm2 region, changing the surface from a long-range 1-D ordered structure to 3-D steps and terraces. Atomic resolution STM revealed ordering of surface point defects along the intrinsic channel direction, with a bias dependence consistent with negatively charged defects migrated to the surface.

As grown sample showed a smooth surface with occasional 0.56 nm steps along b-direction (Fig 9a). As soon as applying DC current (experimentally within 10 seconds), filament like structure with a narrow 0.56nm steps along the b-direction is developed on the terrace. This structure propagates along the b-direction, showing 1D morphology in Fig 9b. This morphology is preserved for a short period of time, but gradually holes with same step height start to form, indicating a random removal of half the unit upon annealing. Careful examination further revealed a step height of 0.15nm shown by a red arrow. This step height matches the height difference between A to B termination, suggesting that a meta-stable surface with A termination shows up after a short DC treatment. With annealing continued, this 1D structure gradually disappears, instead, holes with same step height start to form (Fig.9c). Filament structures are then removed completely, leaving multiple smaller steps on the surface (Fig.9d). In the later part of the annealing, regeneration of new terrace, holes and trenches occur on the surface as seen in Fig.9. Prolonged joule heating again generates trenches on the surface randomly instead of propagating along the b-direction, where the trenches grows both along a(100) and b(010) directions (Fig.9e and 9g). Eventually at least five terrace levels vertically spaced by 0.56nm becomes visible. This implies that significant atomic migration can occur at these temperatures, potentially associated with molecular desorption.

Let us take a closer look at surface atomic structure after Long anneal. Fig. 10 shows atomically flat 4N sample after long anneal (30mins 1100 C). +7 V was applied on the sample, the result of

which is the mapping of empty states on 30 by 30 nm region. It reveals the terraced surface of Ga_2O_3 after anneal, with common step height of 0.56nm. No secondary phase was observed post anneal. On the other hand, regularly spaced ridges are observed along b direction with separation of 0.73nm, which visualizes lattice reconfiguration on the bc plane. The ridge of the superstructure is the center of negative charged defects showing as dark spots or depression on the surface, a lot of which are aligned to the same direction of the ridges, which can be an indirect support of defect chain along b direction, which gets gradually destroyed by high temperature treatment, which was claimed in 1D to 3D polaron hopping mode.

As of the origin of the negatively charged defect, it is natural to think vacuum annealed 4N samples should possess increased number of Vo on the surface, However, Oxygen vacancy formation energy calculations always suggest ε (+2/0) transition levels are well below conduction band minimum, which concludes that Vo always acts as a deep donor, rendering the defect site positively charged, although in some cases neutral states are also energetically favorable (J.B.Varley, 2010) (Lovejoy, 2009). Therefore, the negatively charged defect on the surface should be attributed to either oxygen interstitials or Ga vacancies as intrinsic defect from Frenckel defect formation, and facilitated by annealing. Natural Frenckel defect pair contributes to no change in overall charged state in crystal lattice shown as 2 equations below, however, with migration of defect, adding Oxygen interstitials near surface, or Creation of Ga vacancies (migrating Ga intersitials into the bulk). Surface region can exhibit band bending effect with excessive negatively charged defect accumulated.

$0=V_o^{x+}+O_i^{x-}$ (1)

$0=V_{Ga}^{y-}+Ga_i^{y+}$ (2)

3.2.3 *Electrical conductivity vs annealing time*

The electrical conductivity of single-crystal Ga_2O_3 depends strongly and non-monotonically on annealing history, and is closely related to its surface morphology. To elucidate the effects of annealing, the room-temperature electrical conductivity of the 4N β-Ga_2O_3 samples prepared in various conditions were measured and plotted in Figure.11. Interestingly, the conductivity initially increased with a short heat/current pulse (with in less than 10 seconds), then undergoes a significant decrease with a longer annealing time. This trend is similar in three completely different atmospheres examined in this experiment, suggesting the environment has less influence on the conductivity change, but materials' inherent changes, such as, either phase change, defect migration, lattice reconfiguration, seem to be more responsible.

Let us now correlate the change of electrical conductivity with surface morphology after subjecting to vacuum annealing for different time at 800ºC. It is clear that the increase of conductivity is consistent to the formation of 1D continuous structure which are aligned to b-directions (Fig 9b). However, once the trenches start to form, which physically separates the filaments, the electrical conductivity drops and continues decreased as 1D structure gradually disappears. After 2 hours annealing at 800C, significant reduction of the electrical conductivity occurs with evolution of more complicated 3D terrace structure. At this state, power law analysis of the conductivity shows three dimensional variable-range hopping, indicating increased disorder along the channels, which was also observed from STM.

3.2.4 *Surface electronic state analysis*

Surface electronic structures post different annealing time is summarized in Fig 12.

Ga2p region, which represents sub nano-meter surface composition shows lower Ga_{2p} to $_{O1s}$ ratio in as grown sample compared to annealed samples, which is believed to be caused by sample preparation and incomplete degas, as surface -OH group and environment contaminants were not fully removed during non-joule heating degas procedures. Further annealing does not change Ga2p:O1s signal ratio significantly. This phenomenon can be explained by oxygen defect equilibrium under fixed atmosphere, where the annihilation rate of Vo and lattice O on crystal surface is dictated by annealing temperature and pressure, which in our case remains constant.

Ga_{3d} peaks represent sub-surface compositions of top 3-5 nm of the crystal, translates to 3-4 layers of unit cells of β-Ga_2O_3 in c-direction with ab plane perpendicular to escape depth. As-grown sample shows the strongest Ga_{3d} to O_{1s} ratio, with successive annealing in UHV, the ratio is gradually decreased.

A coarse explanation from the observation to Ga signal decrease, can be an indirect evidence to the migration of Ga vacancies or oxygen interstitials towards the surface, or removal of Ga and injection of Oxygen at vacuum-Crystal interface. It is suggested that the surface defect depletion zone is Ga deficient, opposed to Oxygen deficient from common understanding of reducing atmosphere annealing.

However, when taking a closer look at the data, IT WOULD BE HARD to believe Ga signal decrease is from real stoichiometric redistribution.

Firstly, quantitative analysis of peak under the curve from Ga_{3d} shows that, Ga compositional decay on top surface of the crystal, is as much as 19%, which is regarded as significant deviation from stoichiometry. If it is the case, the top 3-4 layers of unit cells will be significantly distorted with one out of 4 Ga removed from the crystal, and eventually forms new phase incongruently, which is highly unlikely given its chemically stable nature with high melting point.

Secondly, it is being experimentally confirmed that the signal decrease is equivalent to more than 10 monolayers of Ga subtracted from the crystal surface region, which is not consistent with previously reported STM result, in which we neither see metallic Ga on the surface to start with, nor substantial accumulation of Ga vacancies post anneal, instead, only scattered negatively charged defect on the surface was observed.

It can be claimed that the compositional changes are not the first order contributor to Ga signal decrease, with lattice being reconfigured due to elevated temperature, relaxation from interstitial removal, or distortion from interstitial formation. Changes of lattice parameters can alternate the photo electron diffraction pattern, which impacts the photo electron signal in certain takeoff angles, which is called X-ray photoelectron diffraction (XPD). Signal decrease can be from random XPD signal changes post high temperature surface reconfiguration, or nearest neighbor atom changes due to injection of oxygen interstitials.

3.2.5 *Crystal quality from RBS*

Shown in Fig.13 for a regular single crystal, the χmin value is usually less than 10%, however, our virgin crystal shows a χmin value of 18%, suggesting a lower crystal quality, which can be attributed to the occupation of a significant amount of interstitial sites, which contributes to the

scattering of He^+ along the channels. Among two types of negatively charged defects (Oxygen Interstitials, Ga vacancies) which causes surface band bending, oxygen interstitials should post more significant impact to χmin value. During vacuum anneal, due to the surface reducing atmosphere, the migration of oxygen interstitials might be significant enough to scatter across multiple channels, and causes increased scattering of electron conduction along b direction.

3.3 INTERFACE ALTERNATION DEMONSTRATION

Surface states shows significant variations, as well as possible up-ward band bending. When implementing contact to Ga_2O_3 material during future device fabrication, surface alternation will be a huge concern, in a way that contact-material interface change can alter contact barrier height, interface charge distribution or even creation of new interlayers within the device, which causes a further change of electrical response on top of intrinsic electric property alternation. Before realizing Ga_2O_3 into resistive switching device, investigation and understanding of interface alternation during direct current treatment is crucial.

To investigate the interface barrier height change, a piece of Ga_2O_3 was cleaved along (100) plane in air, followed by Ti/Au thermal evaporation deposition under 10^{-8} Torr on one side, and Ni Sputtering deposition on the other side under the same pressure. This sandwich structure intends to create a schottky contact on the Ni side and ohmic contact on the Ti/Au side. Its IV measurement chart was shown in FIG 14, where we put a +/-4V bias to Ni contact, while Ti/Au contact being grounded.

IV measurement at virgin state shows no significant electric signal change after multiple sweeps, suggesting at this voltage, neither Ga_2O_3 intrinsic conductivity nor metal-Ga_2O_3 interface

stoichiometry is being altered by electric current. However, when we heat up the whole schottky assembly with a resistive heater at 150 ºC for 30 min in air, IV character is changed (Purple in Fig.14) that Ni contact is altered from Schottky to non-Ohmic. Further intensive heating at 500 ºC for 10 min makes IV curve close to a straight line(Red), indicating the contact becomes Ohmic after heat treatment.

Contact alternation suggest that the interface between interface condition, as well as surface banding of Ga2O3 is influenced by thermal energy, either by diffusion and agglomeration of defects to the surface, or diffusion of Ni Contact into Ga_2O_3 lattice interstitial sites. Thermal treatment itself generates 2 orders of magnitude change of conductivity before and after treatment, compared to 1 order of magnitude change in intrinsic conductivity change measured by PPMS.

3.4 SUMMARY OF INTRINSIC CONDUCTIVITY STUDY IN GA2O3 SINGLE CRYSTAL

The largest, most surprising result we discovered from single crystal study, is that a two orders of magnitude drop of conductivity is recorded post vacuum annealing. This conductivity drop is independent from surface contact interface, as well as annealing atmosphere, thus not linked to oxygen defect concentration changes. It is a very strong example to claim oxygen vacancy conduction model being fault, and strong support to modeling results proposed by Tracy and Varley.

On top of that, we provided evidences of defect alignment along b direction, by analyzing low temperature conduction following Mott's power law. As grown sample shows 1D hopping dimension which suggests alignment of defect along channel direction. Annealed sample exhibits

3D hopping mechanism, which is attributed to created oxygen interstitials in channeled direction, which results in more scattering.

Scanning Tunneling Microscopy confirms the surface band bending model, with the existence of negatively charged defects observed below surface of the crystal post intensive annealing. Meanwhile, significant atomic migration can be associated.

Moreover, contact improvement on Ga_2O_3 after thermal treatment was observed, whether it is associated with surface reconfiguration of Ga_2O_3 crystal, redox reaction at metal-Ga_2O_3 interface due to elevated temperature, changing surface electronic state, such as band bending, barrier depletion width, Fermi level, and so on, was not identified. However, this portion of research was carried on by another colleague from our group, Hien Pham, in her thesis "Interface barrier height engineering of metal/Ga_2O_3", in which, additional surface state caused Fermi level shift, generated by temperature assisted redox reaction on the surface of Ga_2O_3, was proposed.

Chapter 4. SINGLE CRYSTAL TO PLD FILM

4.1 EXPERIMENTAL GOAL

As introduced in chapter 2, resistive switching is classified into two types, both of which are associated with defect migration under electric field. The agglomeration mechanism of these two have clear difference. In a perpendicularly aligned MIM system, electric field is considered perpendicular, where the contact plane is considered horizontal. Filament is a result of perpendicular stacking of defect, usually as a result of electric breakdown along grain boundaries, with a signature of defect redistribution in horizontal plane. The other mode, interface alternation, is a result of uniform migration of defect perpendicularly, which has little variation of defect concentration horizontally.

Ga_2O_3, with band gap of 4.8eV, expects to sustain a high breakdown electric field based on Baliga's figure of merit [Baliga89], which make it a good candidate for interface alternation resistive switching material.

The uniqueness of beta-Ga_2O_3 crystal surface is investigated in single crystal studies, which can be summarized as follows

1. Ga_2O_3 surface is meta-stable, which exhibits drastic morphological changes post thermal treatment.
2. Surface tends to re-configure, however its impact to conductivity change is unknown.
3. Sporadic negatively charged defects was observed on the surface, which are either Ga vacancies or oxygen interstitials. Increase of this type of defects, will push the surface bending to higher binding energy, while reducing their concentration can reduce it.

Although it is still debatable to claim that in single crystal study, defect is being thermally driven to migrate towards the surface, but we did observe interface state being altered from schottky to ohmic through pure thermal annealing in our experiment, results from an up-ward band bending being changed to flat. Positively charged defects, either Ga interstitials, or oxygen vacancies, were created around metal-Ga_2O_3 interface with the help of thermal stimulus.

In this part of thesis, we would like to repeat the interface barrier height changes, and conduct systematic experiment to probe the cause. Meanwhile, we aim to explore the possibility of interface alternation through electric field. To achieve this goal, we designed a Metal-Ga_2O_3-Metal system with high surface barrier, followed by Electric field treatments, IV measurements and surface characterization.

4.2 BACKGROUND

Our work is inspired by various studies on TiO_x resistive switching [33, 34, 39, 40], in which bi-polar resistive switching was observed from TiOx structure. To investigate the ionic migration, SEM, STEM with the help of compositional analysis such as EDS or TOFSIMS to analyze cross section of interface region around contact at Initial resistance state (IRS), LRS and HRS respectively. As a result, significant atomic variation of Ti:O ratio was observes. From this observation, a push-pull model of oxygen ions migration as a response to external electric field, which controls the localized stoichiometry at metal contact.

Reports of stoichiometric Ga_2O_3 resistive switching were heavily associated with Au [41], Cr [42] diffusion and nanowire structure formation within Ga_2O_3 Host, which can hardly be regarded as resistive switching of Ga_2O_3 itself. Intrinsic Ga_2O_3 switching is only reported in non-stoichiometric

system [43], where crystallization is causing non-stoichiometric phase segregation. This type of switching is not electric field driven, and hardly reversible.

Cu_2O/Ga_2O_3 structure demonstrated reliable switching [44], and was attributed to concurrent filament formation in both Cu_2O layer and Ga_2O_3, although no direct evidence was presented. It would be hard to believe filament formation in Ga_2O_3 based on the fact that Ga_2O_3 is widely used as power semiconductor device, which less likely occurs power breakdown at the similar electric field as Cu_2O. Our studies in Single crystal case shows no evidence of high conductive filament formation laterally with lateral electric field, on contrary, channel direction anisotropy gets easily destroyed during DC treatment. Nevertheless, the thermal energy during lateral DC treatment can cause perpendicular defect migration. Therefore, previously reported resistive switching behavior might be dominantly from Cu_2O filament, associated with interface phenomenon from defect migration in Ga_2O_3 film.

Our work will be demonstrating a fully reversible and repeatable, field driven, bipolar Ga_2O_3 resistive switching in fully oxidized (stoichiometric) Ga_2O_3 film.

To run material characterization, we used Ar-assisted XPS probing which is an even more powerful technique to conduct, compared to STEM-EDS. It generates both lateral and vertical stoichiometric comparison with high accuracy and efficiency. Given significantly different profile fingerprint from filament type agglomeration and interface type agglomeration, we can easily find switching mode type from XPS.

At LRS, defect agglomeration can show up as two distinct binding energy peaks, one being more oxidized(higher binding energy), the other being more metallic(lower binding energy), representing low conductivity regions and high conductivity regions respectively.

In filament type of agglomeration, in which the low conductive state is perpendicular to the surface between top and bottom contacts, low binding energy peak should always exist as we remove the material from top the bottom gradually. On the other hand, for interface agglomeration, low conductivity state is parallel to the contact surface, so the low binding energy peak should reach a maximum as we reach the interface, and quickly decrease to none as we probe deeper.

4.3 EXPERIMENTAL

4.3.1 *Pulse Laser deposition (PLD)*

As Ga_2O_3 is very sensitive to defect concentration, and material performances is heavily related with dimension factors like thickness, contact width, surface smoothness, and so on, product purity, chemical and dimensional uniformity though out the film is crucial to the success of this study. Ultra High Vacuum Pulsed Laser Deposition (PLD), becomes a technique suitable for this study as it is a reliable oxide deposition technique with fine control of deposition conditions and evaporation rate, yet with little impurity introduction if the target material is carefully selected.

4.3.1.1 Basic Setup of PLD

A pulse laser deposition (PLD) system with coherent KrF(248 nm) excimer laser was used for thin film deposition. The deposition chamber base pressure was 2E10-8 Torr, and the laser beam was directed into the chamber through a set of optical mirrors and a focus lens, and the laser injection

angle was 45˚ to the horizon. The laser and optical path was carefully calibrated so that a 2mm*20mm laser spot is focused on a rotatable 6-target holder placed horizontally at the bottom of the chamber. A substrate holder was installed 10cm above the target holder, and the substrate holder edge was directly above the laser spot where plume is generated during growth. A SiC heater was placed to the back of the substrate holder so the substrate can be heated resistively during the deposition up to 1100 ºC. In addition to the PLD setup, the chamber also has two magnetron sputtering guns installed which was aligned to the center of the sample with the target to sample distance of 30cm.

4.3.1.2 Versatility of PLD

In pulse laser deposition, film properties are strongly influenced by several important factors, such as growth environment, deposition rate, plume geometry and substrate temperature. These factors can be separately controlled during Pulse laser deposition. Firstly, growth environment can be altered by injecting 99.99% O2 or Ar gas into the chamber, where the flow rate is controlled by Mass Flow controllers (MFC). Besides MFCs, Chamber pressure is further controlled by computer controlled pneumatic valve between Turbo pump and UHV chamber, by adjusting the pumping conductance, the pressure of the chamber can be maintained at set point when a constant flow of gas is introduced. Secondly, laser parameters, such as fluence, repetition rate and pulse duration, can be changed to vary the deposition rate and plume geometry, which can be further modified by changing the sample-to-target distance.

4.3.1.3 Device fabrication using PLD and Magnetron Sputtering

With above mentioned set up, we developed a technique to fabricate a smooth Ga_2O_3 film with arrays of top and bottom contacts, allowing efficient production of small sized resistive switching cell in sandwich structure. Electrical measurement and direct current treatment of the film through out of the plane direction.

Preferred cell structure is a complete metal film on a 2 inch Si wafer as bottom contact, which allows easy grounding during IV measurement. Second layer is stoichiometric Ga_2O_3 film with uniform thickness as resistive switching medium. Top layer is patterned top contact arrays with reduced contact sizes. In this way, each top contact, together with Ga_2O_3 and bottom electrode beneath it, forms a millimeter sized resistive switching cell. Depending on the size of top contacts, and designed contact to contact separation, hundreds of identical switching cells can be fabricated. Asymmetrical top and bottom contacts can be fabricated to create a schottky device, after stimulus is applied, the change of material conductivity and contact alternation can be reflected by electrical output.

In this experiment, a commercial β-Ga_2O_3 target of 99.999% purity was mounted on the sample holder and pre-ablated by laser for 5 min in $2E10^{-8}$ Torr base pressure. Meanwhile, an Ir and Ni target was installed in 2 sputtering gun and pre-sputtered at 30W in 10mTorr Ar for 10 min prior to deposition.

10 min 20W sputtering deposition of Ir over layer was done at 10mTorr Ar without heating the substrate. Succeeding Ga_2O_3 film deposition was done in 10mTorr O2 pressure at room temperature. To further ensure the film uniformity, substrate was rotating at 20 Round per minute (RPM) during deposition, and target was rotating and rastering for uniform target ablation and minimum change of plume geometry/composition. Experiments were done in 10Hz laser repetition rate with $150mJ/cm^2$ laser fluence. After 2.5 hours (100000 pulses) of deposition, sample is

transferred out of the chamber and a mask with uniform hole-array, on which the size of each hole is 0.5mm*0.5mm mesh size and separation between holes is 1mm, is mounted in front of Ga_2O_3 layer. Then, sample is re-inserted back to the UHV chamber and 100 ºC annealing for 15 min is carried out to remove the substrate contamination. 1 hour is waited after annealing to ensure sample is cooled down to room temperature, then top contact is deposited with 20W sputter gun power in 10mTorr of Ar.

As a result, an array of Ga_2O_3 switching cell is fabricated (Top view of one array of cells is shown in Fig 15). Each cell is 0.5 mm in length and width, with a sandwich structure of 100nm of Ni as top electrode, 100nm of Ga_2O_3 as interlayer, 150 nm of Ir as bottom electrode on top of Si substrate. Ni and Ga_2O_3 thicknesses were confirmed with a Profiler scan shown in Fig. 16. Film properties under weak to strong external field was characterized using IV measurement, XRD and XPS.

4.3.2 *Electrical switching Experimental*

Electrical measurement was carried out on as deposited cell using an electrical probe station. This stage has probe connected to the top electrode, with bottom electrode grounded. Top electrode probe is connected to Keithley power source which can generate voltages from -30 to +30V with the finest increment of 0.01mV. An amp meter is connected in electrical loop for current measurement. Voltage applied to top electrode, and respective current changes were recorded. Same stage was used to apply large external field in attempts to electrically alter the structure.

For virgin sample, as Ni-Ga_2O_3 forms typical n-type schottky contact (Fig 17). When applying positive bias to the top contact, Ni to Ga_2O_3 is subjected to a forward bias, Fermi energy of Ni is

lowered with respect to the Fermi energy in n-type Ga_2O_3 showing in Fig 18(a). This results in a smaller potential drop across the semiconductor. The balance between diffusion and drift is disturbed and more electrons will diffuse towards the metal than the number drifting into the semiconductor. This leads to a positive current through the junction at a voltage comparable to the built-in potential. As a negative voltage is applied (Figure 18 (b)), the Fermi energy of the Ni metal is raised with respect to the Fermi energy in the semiconductor. The potential across the semiconductor now increases, yielding a larger depletion region and a larger electric field at the interface. The barrier, which restricts the electrons to the metal, is unchanged so that the flow of electrons is limited by that barrier independent of the applied voltage.

4.3.3 *XRD*

Samples were put on BRUKER 2D XRD system with X-ray spot size smaller than 0.5mm in diameter. X-ray is aligned to the center of the subject cell carefully during each scan so that each scan only contains crystal structure information of a single Ir/Ga_2O_3/Ni cell. Virgin sample and Ohmic sample are scanned separately, while ohmic sample is mounted with a Keithly Voltage source connected to the top Ni contact with bottom Ir contact grounded to simulate external bias applied to the material during IV measurement environment. After first XRD scan, Ohmic sample were subjected to +/-10V and +/-30 volt voltage sweep, followed by another XRD scan at exactly the same spot.

4.3.4 *Ar ion Sputtering assisted XPS*

Our sole interest is the differences in stoichiometry, electronic states of Ga, O, Ni at Ni/Ga_2O_3 interface before and after the sample being exposed to external stimulus. However, as introduced in 4.3.4, X-ray Photoelectron Spectroscopy is a surface sensitive technique due to 2-5nm escape depth of photoelectrons. In our cell structure, Ni-Ga_2O_3 interface is buried underneath 100-150 nm of Ni top contact, rendering difficulties to use XPS to probe the interface. Ar sputtering is used to remove Ni top electrode. A flux of Ar ions is focus to top surface of the sample in XPS chamber, with flux profile of 0.5 by 0.5mm, the center of the Ar flux is carefully calibrated to be the same as the center of Al K alpha X-ray. X-ray is set at 45 degree incident angle to the sample surface, with spot size is set to be 100 by 100 microns. Sputter gun power was set to 2kV 1mA in which Ni was sputtered off at a rate of approximately 2nm/min. Sample was pre sputtered for 40 mins, then Ga_{2p}, Ni_{3p} and O_{1s} spectrum were taken after every 30 seconds of sputtering, with estimated 0.5nm removal per cycle. Each peak was carefully deconvoluted to and area under the curve was calculated, then plotted against sputtering cycles.

4.4 DATA ANALYSIS AND DISCUSSION

4.4.1 *Electrical switching experiment*

Virgin sample IV curve was shown in Fig 19. Although the schottky IV loop confirms what we expected (Fig 18), a small hysteresis was observed in the loop. As bias started from 0 V to positive region, current density remains almost undetectable until bias reached 2.3V which was the contact barrier height. Current linearly increases until reaching bias limit 10V. However, current density during ramp down does not follow the ramp up curve. Instead, 20-50% higher current intensity is recorded until reaching 2.3V, as device turns into higher conductivity state compare to original state during ramp up. When ramping down, the tunnel current signal also follows a high current density line at first, when hitting -10V and gradually step down to -8V, current density slowly decreases, as the device is switched back to low resistance state until whole IV loop is completed. This process is highly reliable and repeatable, as shown in blue curve after 5 switching loops.

Similar cases was observed in other diode studies [4], shown in Fig.20, that a hysteresis IV loop with about 5% offset is often observed with high current density(10^{-2}A/cm^2) IV loop. The current offset is believed to be either variation of carrier density, due to a slight lowered device temperature during ramp up process. However, in our case, even with a 5 orders of magnitude smaller current density, i.e., providing less thermal variation to the device, the hysteresis offset is 5-10 magnitudes larger, suggesting carrier density increase is beyond thermal activation region. Assumption is made that larger variation in the conductivity can be attributed from defect redistribution and agglomeration under bias, brings along intrinsic electrical property alternation. In this case, contact condition remains unchanged, as the barrier height remains 2.8eV at both HRS and LRS states.

Another new cell is picked to receive larger external field. It is discovered that after applying -30V bias(-3E8V/m electric field) to the sample, recorded current density jumps from 10-7 A/cm2 to of 10-4 A/cm2. Following IV measurement shows the electrical pulses changed the contact behavior from schottky to complete ohmic shown in Fig.21.

Further IV characteristics analysis were carried out on this cell, shown in Fig.22.

First measurement was done using -5E7 to +5E7 V/m electric field loop, and no significant resistive switching behavior was observed. After increasing the electric field magnitude from 5E7 V/m to 2E8 V/m, a clear difference in high resistance state during ramp up and low resistance state during ramp down was observed. Meanwhile, the IV loop remains symmetric, indicating Ni/Ga_2O_3 interface remains ohmic during the entire switching time. The first two sweeps can be repeated up to 30 times with no sign of degredation. A more significant change in IV loop was observed after increasing the field density from 2E8V/m to 3E8V/m, as when electric field reached from -3E8 V/m to -1.3E8V/m, electrical current exhibits a sharp drop by 2 orders of magnitude. From -1E7V/m to 3E7V/m, film remained at high resistance state with asymmetric IV curve. Ramp down loop from +3E8 V/m to -3E8 V/m, film was switched back to low resistance state with symmetric IV characteristics. This characteristic resistive switching is highly unstable, which can only be repeated 1-5 times on each cell, ended with pure schottky contact which could not be switched back to ohmic with further voltage sweeps.

In the resistive switching experiment, 3 distinct states were shown which may be caused by crystal structure formation, as well as interface alternation.

1st state is named virgin state, when the cell is not subjected to strong electrical field. A repetitive schottky IV curve can be observed.

2nd state is named Ohmic state, when the cell is subjected to +30V bias(3E8V/m electric field). The Ni/Ga_2O_3 is altered from Schottky to Ohmic.

3rd state is the schottky state during -30V to +30V sweep at 2nd state, when the ohmic contact was altered back to schottky when the voltage reached -10V(-1E7V/m).

4.4.2 *XRD at different states*

Shown in Fig.23, As deposited film was in amorphous state. After subjected to external bias, both Rhombohedral (α-phase) and Monoclinice (β-phase) Ga_2O_3 were observed. According to Lakshmi Nagarajan's group's annealing data in which β-Ga_2O_3 starts to crystallize at 633K, 3E8V/m external field can introduce substantial joule heating effect which increases the film temperature higher than 633K in our system. However, the crystallization should not be contributing to the creation of Ga rich and Ga deficient phase since initial Ga_2O_3 film and formed β-Ga_2O_3 phase was all stoichiometric.

10 V sweep and 30V sweep shows similar impact to sample crystallinity, that a continuous growth of beta-Ga2O3 (400), (401) and (002) plane was observed. This again confirms the growing crystallinity would not facilitate Ga rich amorphous phase formation, thus yield little impact to film conductivity, as no conductivity change was recorded after multiple 10V sweeps.

4.4.3 *Ar assisted XPS depth profiling and Quantitative analysis using Beer-Lambert law*

Beer-Lambert law is used to simulate the film stacks, and how different components moves with respect to probing depth after treatment. For an electron of intensity, Io, emitted at a depth, d, below the surface, the intensity is attenuated as formula below.

$Is= Ioexp(-d/\lambda)$

In this study, we propose a layered structure based on XPS experimental result. And calculate and integrate $Is= Ioexp(-d/\lambda)$ of each component, assuming λi , the inelastic mean free path, is 10ML. Then we remove the top monolayer component from proposed structure, and do Is Calculation again. By repeatedly removing top monolayer from modeled structure, we can plot the simulated Signal intensity vs Depth, and compare it with real data. Any disagreement between simulated result and experimental result was discussed and investigated, so that a new, more realistic film stack is re-proposed and simulated again, until simulated result matches with experimental data.

4.4.3.1 Virgin state (1st state)

XPS profile scan (Fig.24a) shows after 40 mins of pre-sputtering top Ni contact of the sample is still not completely removed, however, Ga2p peak has shown (Fig.25a), suggesting top Ni contact is thinner than Ga2p electron escape depth. In this case, Ga_{2p} peak contains information of Ga_2O_3 film at interface, which is not being damaged by Ar ion bombardment. Virgin sample shows distinct Ni/Ga_2O_3 interface, illustrated in Fig 25, Post 1st cycle of pre-sputter etch, where metallic Ni was still on the surface, 2 peaks can be deconvoluted from Ga_{2p} signals, with binding energy of

1118eV and 1116.7eV, which corresponding to Ga^{3+} and Ga0. After another cycle of Ar sputter etch, metallic Ga peak is gone together with significantly reduced Ni signal. Suggesting the metallic Ga is at Ni/Ga_2O_3 interface. The metallic Ga observed is not believed to be caused by redox reaction from Ni deposition, in which case Ni may take away oxygen from Ga_2O_3 film, leaving some metallic Ga on top. This reaction is less likely to occur at room temperature, supported by binding energy of Ni_{3p} post Ar sputter cycle 2 (Fig.24), where it shows no oxidation state of Ni at Ni/Ga_2O_3 interface, as no binding energy shift of Ni_{3p} peak was observed. One explanation to the metallic Ga layer was long pre-sputter etch elevated the temperature of material which facilitate small scale of Ga interstitial migration and agglomeration on top surface of Ga_2O_3.

Further sputtering completely removed Ni top contact, resulting a slight shift of Ga peaks in XPS spectra to higher binding energy due to worse charge dissipation without metallic over layer. However, the overall peak shape remains the same, indicating Ar sputtering is not changing Ga electronic state.

4.4.3.2 Ohmic state (2nd state)

Similar to Virgin sample, Ga(0) metallic state and Ga^{3+} state is also observed at Ni/Ga_2O_3 interface, . However, the intensity of Ga(0) signal is larger, which lasts 40 sputtering cycles before disappear (Fig 27), suggesting -30V bias is driving metallic Ga towards Ni-Ga_2O_3 interface, and eventually caused large degree of metallic Ga segregation. Single crystal study suggests this segregation can be purely thermal driven, however, a Ga depletion zone should be created at sub-surface region, however, it is not observed in this case. Another possible cause of Ga segregation is ionic migration

of Ga3+ towards interface due to negative bias applied to the surface, or O2- migrate deeper to the film, leaving an Oxygen depletion/Ga enriched region on the surface.

We have simulated 2 stacks. One of which is with distinct Ni/Ga/Ga2O3 interface, while other stack has 15ML of interdiffusion layer between Ga and Ni. The Ga peak fits well to real data in either case, when the difference lies within Ni tail in models with 15 ML interdiffusion, which fits better to our observation. The subtle Ni Diffusion should be concentration gradient driven from Ni contact to deeper film structure, as opposed to Ga ionic migration which is field driven, with diffusion vector pointing towards the surface.

4.4.3.3 Schottky state (3rd state)

Same as characterizing ohmic "on" state film, XPS profile was carried out on Resistive Switched "Off" film when the conductivity dropped from 2 orders of magnitude at which it starts to behave in schottky IV curve. Instead of having 2 peaks at interfaces spectrum, only one peak at 1118.0eV was observed as shown in Fig.29, which is neither fully oxidized Ga^{3+} state(1118.5eV), nor Ga(0) metallic state(1116.7eV). By looking at O_{1s} spectrum, it is clear that O1s peak is also shifted to a lower binding energy, so the entire Ga_2O_3 is bending to lower binding energy at surface. So we still regards the peak at 1118.0eV as Ga_{2p}(3+). As sputtering cycle increases, the peak representing Ga3+ state increased its intensity. Meanwhile, its binding energy gradually shifted higher. The biding energy of the main peak was recorded as 1118.0, 1118.2, 1118.4 and 1118.5eV with increasing sputtering cycles. A clear Ga0 metallic peak at 1116.5eV started showing after 20 cycles of sputtering, and became significant post 30 cycles of sputtering.

The fact that metallic Ga peak was not observed until 20 cycles of Ar sputtering was conducted, suggests unique Ga_2O_3/Ga/Ga_2O_3 sandwich structure was formed at this state. Confirmed by simulation in Fig 34, that as many as 15 ML of Ga(0) was buried under 5ML of Ga_2O_3. This is a direct evidence that by applying negative bias to top contact, metallic Ga is being driven to deeper region of the cell, making Ga_2O_3 interface back to schottky type Ni(O)-Ga_2O_3 contact.

Metallic Ni diffusion, is confirmed to be further diffused into Ga_2O_3 Modeled in Fig 31. It confirms our prediction that this diffusion is concentration driven, and independent from external electric field. However, "metallic" Ga Species behaves differently. When surface is positively charged, it is diffusing out of the surface, and creates a Ga rich region at Ni-Ga2O3 interface. However, when surface is negatively charged, metallic Ga species were diffused deeper into Ga_2O_3, leaving top surface GaO_x.

On the side note, another effect observed from this sample is Ni contact being heavily oxidized starting from top surface. Data and simulation (Fig 31) both shows metallic Ni was preserved at Ni-Ga_2O_3 interface. This is a sign of degradation of film stack from top to bottom from environment oxygen when operating at elevated temperature.

4.4.4 *Quantitative analysis using Schottky emission equation*

Ar Assisted XPS results suggest Ga(0) layer is the effective switching layer. We determined the Ga(0) layer thickness is about 15ML(~8nm) based on simulation using Beer-Lambert law. On the other hand, we can roughly calculated the thickness of this layer using Schottky emission equation, Schottky emission equation

Schottky emission equation

$$J = AT^2 \exp\left[\frac{-(W - \Delta W)}{kT}\right]$$

Where A is a universal constant, k is Boltzmann constant. W is local work function, ΔW is electric field modified work function in

$$\Delta W = \sqrt{\frac{e^3 F}{4\pi\varepsilon}}$$

ε is the permittivity of Ga2O3, and F is the local electric field, which can be further represented by V/d, where d is the effective thickness of switching layer,

$$J = AT^2 \exp\left[\frac{-e\left(\varphi - \sqrt{eV/4\pi\varepsilon d}\right)}{kT}\right]$$

By plotting $\mathrm{Ln}\left(\frac{J}{T^2}\right)$ vs $V^{0.5}$, we can get slope value of $\sqrt{\frac{e^3}{4\pi k^2 T^2 \varepsilon d}}$. By borrowing single crystal data from Fig 7, we can solve for d, which is around 1.93. Estimated effective thickness of Ga layer is 14.8 nm, which is close to our simulation estimation ~8nm.

4.5 SUMMARY

We successfully demonstrated a unique bipolar resistive switching in Ni/Ga_2O_3/Ir structure, with voltage bias applied to Ni contact, while Ir contact is grounded. Initial Resistance State demonstrated Schottky diode behavior, given a high contact barrier between Ni-Ga_2O_3. After -3E8V/m forming electric field.

The contribution of large forming current/field can be two-folded. Firstly, the thermal impact from strong electric pulse is considered substantial, based on XRD, which shows crystallization of

Ga_2O_3 after pulse, suggesting the local temperature was higher than crystallization temperature 623K. This degree of thermal treatment can cause agglomeration of defect at the interface based on our single crystal study. Secondly, despite the thermal impact, large external electric field can be another driving force to cause migration of positively charged defects towards negatively biased surface. The candidates for positively charged defects are Ga interstitials or Oxygen defects. Unfortunately, it is yet to identify the formation of metallic Ga layer is due to Ga interstitial agglomeration, or Oxygen depletion.

With interface barrier drops, sample is switched to LRS, which follows Ohmic conduction behavior. When sample is subjected to positive voltage bias, as shown in FIG 31 case 1, a reversed defect migration was expected, therefore interface is changed back to stoichiometric, and conduction mechanism is switched back to Schottky. When we reduce electric field from 30 to -13V, a Gradual Schottky to Ohmic transition was observed with voltage onset of about -5V, as shown in FIG 13 case 2. It is suggested that positively biased top surface is driving Ga rich interface upward, alternate Ni-Ga_2O_3 back to Ni-GaO_x-Ga_2O_3 interface.

The interface alternations were not only speculated based on IV measurements, but also experimentally confirmed using Ar-Sputter assistive XPS depth profiling and film stack modeling. Although we can repeat Schottky-Ohmic resistive switching on multiple devices, its repeatability within single device is limited to only up to 5 times. XPS analysis suggests the device is subjected to heavy oxidation due to high working temperature in ambient environment, which can be detrimental to Ni Contact and Ga functional layer, as a result, fast degradation of the device is observed.

Chapter 5. FUTURE EXPERIMENTS

5.1 XPD

One of the major controversy in the thesis is the interpretation to angle resolved XPS from Chapter III, as stated before, the Ga signal decrease is as much as 16%, which is hard to attribute the signal decrease to stoichiometric change alone. In general understanding, this degree of stoichiometric change should have caused phase segregation, and showed up as emerging of new Ga_{2p} peak. The fact that we still see single phase beta-Ga_2O_3 can be either its tolerance to interstitials is extremely high, which needs further modeling support. A more possible explanation is large signal changes was from photo electron diffraction effect. The intensity of excited photoelectron is not only determined by number of photo electron being excited from X-ray, but also distributed as a function of azimuthal or polar angle of sample, due to photo diffraction effect from neighboring atoms. During surface relaxation and re-configuration, XPD pattern will be changed accordingly with the changes of bond length and bond angles in top monolayer of the atoms. In our STM atomic resolution scans, surface congregation along b direction is directly observed. As a result, with proper placement of analyzer angle, we can observe signal intensity changes due to reduced electron diffraction along a specific direction. To fully understand it, fixed angle scan is not sufficient. Instead, full azimuthal or polar angle scan before and after annealing can provide us with how XPD pattern has drifted due to surface reconfiguration, and give us a more reliable interpretation to the root cause of Ga signal decrease.

5.2 TUNING OF FILM THICKNESS AND EXTERNAL FIELD STRENGTH

By using mono-valent transition metal as resistive switching material is that it is hard to find an intermediate state between fully ionized cation and neutral metallic state, compared to multi-valent metals like Ti and Ni. To create a stable low conductivity state, so far there is no other method but to form a close to metallic state where almost all oxygens are deprived from lattice, which requires sufficient amount of energy from external stimulus to form and cure. This is the fundamental reason for lack of repeatability in our prototype resistive switching devices, that large energy injection can easily degrade interfaces. Our resistive sweeping was only a prove of concept that field driven defect agglomeration can be achieved, but we failed to control the degree of Ga agglomeration, resulting in a thicker than needed active layer formation, with close to metallic Ga(0) state formation. It is still believed that surface band bending can be controlled by adjusting surface defect concentration, which causing phase segregation, so an intermediate high conductivity state can be found. Therefore, a more systematic design of experiment in terms of incremental increase of external stimulation will be interesting. Meanwhile, even with aggressive phase segregation, the proposed effective switching region is still at 8-16 nano-meter scale, which means in new experiment, a thinner, smaller scale of switching device can be fabricated. Smaller scale device can substantially decease the forming voltage needed, which should reduce the unnecessary joule heating in the system.

5.3 ANTI-OXIDATION FOR REPEATABILITY IMPROVEMENT

Another proposed structure improvement to current Ni/Ga_2O_3/Ir system is to replace top Ni contact with other schottky oxide contact, such as ITO, which can sufficiently reduce the degradation on top contact from surface oxidation.

BIBLIOGRAPHY

1. *Bermudez, V.M., The structure of low-index surfaces of Beta-Ga2O3. Chem. Phys. , 2006. 323: p. 193-203.*

2. *E G Villora, K.S., Y Yoshikawa, etal, Electrical conductivity and carrier concentration control in β-Ga2O3 by Si doping. Applied Physics Letters 2008. 92: p. 202120.*

3. *T. C. Lovejoy, E.N.Y., N. Shamir, J. Morales,E. G. Villora, K. Shimamura, S. Zheng, F. S. Ohuchi, and M. A. Olmstead, Surface morphology and electronic structure of bulk single crystal beta Ga2O3. App. Phys. Lett., 2009. 94: p. 081906.*

4. *D. P. Halliday, J.M.E., P. N. Adams, E. R. Holland and A. P. Monkman, A visible large area Light Emitting Diode Fabricated from porous Si using conductive polyaniline contact. IEE Colloquium on Materials for Displays, 1995. 13: p. 131-136.*

5. *Tippins, H.H., Optical Absorption and Photoconductivity in the Band Edge of β-Ga2O3. Phys. Rev. A 1965. 140: p. 1A.*

6. *Z. Ji, J.D., J. Fan, and W. Wang, Gallium oxide films for filter and solar-blind UV detector. Opt. Mater. , 2006. 28: p. 415.*

7. *T. Oshima, T.O., N. Arai, N. Suzuki, H. Hino, and S. Fujita, Flame detection by a β-Ga2O3-based sensor. Jpn. J. Appl. Phys. , 2009. 48(Number 1R).*

8. *GW Paterson, J.W., D Moran, R Hill, AR Long, I Thayne, M. Passlack, R. Droopad, Gallium oxide (Ga2O3) on gallium arsenide - A low defect, high-K system for future devices. Mat. Sci. Eng. B, 2006. 135: p. 277-81.*

9. *Tomm, Y.K., J.M.; Yoshikawa, A.; Fukuda, T., Floating zone growth of β-Ga2O3: a new window material for optoelectronic device applications. Solar Energy Materials and Solar Cells 2001. 66(1-4): p. 369-374.*

10. *Shimamura, K.V., E.G.; Domen K, Yui K; Aoki, K.; Ichinose, N., Growth and characterization of beta-Ga2O3 single crystals as transparent conductive substrates for GaN. Physics and Simulation of Optoelectronic Devices XIII, 2005. Proc. SPIE 5722(380).*

11. *M. Fleischer, J.G., H. Meixner, H2 -induced changes in electrical conductance of β-Ga2O3 thin-film systems. Applied Physics A, 1992. 54(6): p. 560-566.*

12. *Meixner, M.F.a.H., Oxygen sensing with long-term stable Ga2O3 thin films. Sensors and Actuators 1991. B5: p. 115-19.*

13. *P. Gollakota, A.D., P. Wellenius, P. L.M. Lunardi, J. F. Muth, Y. N. Saripalli, H. Y. Peng, H. O. Everitt, Optical characterization of Eu-doped beta-Ga2O3 thin films. App. Phys. Lett., 2006. 88(221906-1-3).*

14. *Higashiwaki, e., Depletion mode Ga2O3 metal oxide semiconductor field-effect transistors on beta-Ga2O3 substrates and temperature dependence of their device characteristics. App. Phys. Lett., 2013. 103: p. 123511.*

15. *Adachi, K.S.a.S., (Tb3+, Eu3+)-Codoped Ga2O3 Phosphors: Synthesis and Photoluminescence Properties. J. Solid State Sci. Technol. , 2016. 5(5): p. 67-73.*

16. *Lorenz, M.R., Woods, J. F. and Gambino, R. J., Some Electrical properties of the semiconductor beta-Ga2O3. J. Phys.Chem. Solids, 1967. 28(3): p. 403-404.*

17. *D.Gourier, L.B.a., Origin of Blue illuminescence of beta-Ga2O3. Journal of Physics and Chemistry of Solids, 1998. 59(8): p. 1241-1249.*

18. *M.Bartic, e., β-Gallium Oxide as Oxygen Gas Sensors at a High Temperature. Journal of American Ceramic Society, 2007. 90(9): p. 2879-2884.*

19. *T. C. Lovejoy, R.C.X.Z., E. G. Villora, K. Shimamura, H. Yoshikawa, Y. Yamashita, S. Ueda, K. Kobayashi, S. T. Dunham, F. S. Ohuchi and M. A. Olmstead, Band Bending and Surface defects in beta-Ga2O3. App. Phys. Lett., 2012. 100: p. 181602.*

20. *JB Varley, e., Oxygen vacancies and donor impurities in beta-Ga2O3. App. Phys. Lett., 2010. 97.*

21. *E. G. Villora, K.S., T. Uljie, K. Aoki, , Electrical conductivity and lattice expansion of beta-Ga2O3 below room temperature. Appl. Phys. Lett. , 2008. 92: p. 202118.*

22. *M. Yamaga, G.V., K. Shimamura, N. Ichinose, M. Honda, Donor structure and electric transport mechanism in β-Ga2O3. Physical Review B 2003. 68.*

23. *Denninger, H.J.K.G., The oxygen vacancy in β-Ga2O3: a double resonance investigation. Mag. Res. In Chem., 2005. 42: p. S145-152.*

24. *E. G. Villora, M.Y., T. Inoue, S. Yabasi, Y. Masui, T. Sugawara, T. Fukuda Optical spectroscopy study on β-Ga2O3. Jpn. J. Appl. Phys. , 2002. 41: p. L622-5.*

25. *T. Harwig, G.J.W., and G. J. Dirksen, Electrical properties of β-Ga2O3 single crystals. Solid State Commun. , 1976. 18(9-10): p. 1223-1225.*

26. *CHANG W Y, L.Y.C., WU T B, et al. , Unipolar resistive switching characteristics of ZnO thin films for nonvolatile memory applications. App. Phys. Lett., 2008. 92(2): p. 022110.*

27. *TERABE K, H.T., NAKAYAMA T, et al. , Quantized conductance atomic switch. Nature, 2005. 433(7021): p. 47-50.*

28. *SZOT K, S.W., BIHLMAYER G, et al. , Switching the electrical resistance of individual dislocations in single-crystalline SrTiO3. Nature Materials, 2006. 5(4): p. 312-320.*

29. *LEE M J, S.S., KIM D C, et al. , A low-temperature-grown oxide diode as a new switch element for high-density, nonvolatile memories. Journal of Adv Mater, 2007. 19: p. 73-76.*

30. *TSUNODA K, K.K., NOSHIRO H, et al. , Low power and high speed switching of Ti-doped NiO ReRAM under the unipolar voltage source of less than 3 V. IEEE International Electron Devices Meeting, 2007: p. 767-770.*

31. *INOUE IH, Y.S., AKINAGA H, et al. , Nonpolar resistance switching of metal/ binary-transition-metal oxides/ metal sandwiches:homogeneous/ inhomogeneous transition of current distribution. J. Phys Rev B, 2008. 77: p. 035105.*

32. *KWON D H, K.K.M., JANG J H, et al. , Atomic structure of conducting nanofilaments in TiO2 resistive switching memory. J. Nat Nanotechnol, 2010. 5: p. 148-153.*

33. *CHAE S C, L.J.S., KIM S, et al. , Random circuit breaker network model for unipolar resistance switching. J. Adv Mater, 2008. 20: p. 1154-1159.*

34. *YANG Y C, P.F., LIU Q, et al. , Fully room-temperature-fabricated nonvolatile resistive memory for ultrafast and high density memory Application. J.Nano Lett, 2009: p. 1636-1643.*

35. *XU N, L.L., SUN X, et al., Characteristics and mechanism of conduction/set process in TiN/ZnO/Pt resistance switching random-access memories. App. Phys. Lett., 2008. 92: p. 232112.*

36. *Zinkevich, M.A., F, Thermodynamic assessment of the gallium–oxygen system. J. Am.Ceram. Soc. , 2004. 87(4): p. 683-691.*

37. *A.S. Skal, B.I.S., , Fiz.Tverd, Mott equation for low temperature hopping conductivity. Sov. Phys.-Solid State 1974. 1190.*

38. *Shklovskii, A.L.E., Electronic properties of doped semiconductors. Springer series in Solid State Science, 1984. 45.*

39. *Iulia Salaoru, e., Resistive switching of oxygen enhanced TiO2 thin-film devices. App. Phys. Lett., 2013. 102.*

40. *Huang, Y.-J.e.a., Dual-functional Memory and Threshold Resistive Switching Based on the Push-Pull Mechanism of Oxygen Ions. Sci. Rep., 2016. 6: p. 23945.*

41. *Hsu CW, C.L., Bipolar resistive switching of single gold-in-Ga2O3 nanowire. Nano Letter, 2012. 12(8): p. 4247.*

42. *Tseng, D.-Y.L.a.T.-Y., Forming-free resistive switching behaviors in Cr-embedded Ga2O3 thin film memories. J. Appl. Phys. , 2011. 110: p. 114117.*

43. *Manfred Martin , R.D.E., Thermodynamics, structure and kinetics in the system Ga–O–N. Progress in Solid State Chemistry 2009. 37: p. 132-152.*

44. *Y. S. Zhi, P.G.L., etal. , Reversible transition between bipolar and unipolar resistive switching in Cu2O/Ga2O3 binary oxide stacked layer. AIP advences, 2016. 6(015215).*

VITA

Xiaohao (Sam) Zheng
Ph.D Candidate
46940 Masonic Terrace
Fremont, CA, 94539
Tel: (206)446-4261(c)
Email: Xiaohao.Zheng@wdc.com

EDUCATION

UNIVERSITY OF WASHINGTON
Seattle, WA
Ph.D. Candidate in Materials Science and Engineering

- Thesis: β-Ga2O3: a Transparent Conductive Oxide for potential resistive switching application
- Advisor: Dr. Fumio Ohuchi
- GPA: 3.54

SICHUAN UNIVERSITY Chengdu, China
B.S. in Materials Science and Engineering --- Sept 2007

UNIVERSITY OF WASHINGTON
Seattle, WA
Exchange Student in Materials Science and Engineering --- Sept 2005-2006

WORK EXPERIENCE

Staff Engineer Process Development 2013.8 - present

- Serve as an architect to design and develop integrated wafer processes/process flow for Heat Assisted Magnetic Recording (HAMR)
- Integration Engineer owner responsible for qualifying building blocks for HAMR device
- Work with design and program teams to understand optical & magnetic requirements; translate these needs to physical requirements in wafer processes
- Work with module process development and manufacture engineering teams to develop processes to satisfy design requirements
- Manage and control WIP for process/product development; set up process route for product and process development
- Collect and analyze data from QST, TEG, assembly, test, and drive build; correlate the performance to wafer processes
- Identify processes and parameters improvement needs; drive the improvement plans to satisfy customer needs.

RESEARCH EXPERIENCE

University of Washington (Sept. 2007-June 2013)
Seattle, WA
Research Assistant - Micron Laboratory, Department of Materials Science and Engineering,
Condensed Matter physics Laboratory, Department of Physics

- Growth of thin film Ga2O3 into preferred structure and geometry; Its contact material selection and interface analysis, and development of solar Blind prototype memristic device based on Ga2O3
- Doping Transition Metal Cr and Mn into Ga2O3 for Dilute Magnetic Semiconductor(DMS) study
- Optimization of thin film Ga2O3 growth in physical and chemical vapor depositions
  - Sol-gel synthesis of Ga2O3, followed by spin coating and annealing for polycrystalline β-Ga2O3
  - Metalorganic Chemical vapor deposition using Trimethylgallium as precursor on GaN substrate
  - Magnetron Sputtering using polycrystalline Ga2O3 target
  - Pulse Laser Deposition on various substrates in different environments
- Metal-Ga2O3 interface crystalinity, stoichiometry, morphology and electronic analysis

Patent Disclosure/Trade secret

- Western Digital Disclosure #8525, "A Method To Do Aggressive Material Removal From The Bottom Of Trench Structure With Pristine Structure In The Field Preserved" Xiaohao Sam Zheng, Dujiang Wan, Jinwen Wang, Tsung-Feng Wu and Jerome Marcelino
- Western Digital Disclosure #8383, "A Method To Protect Writer Pole From Corrosion For HAMR Head" Tsung-Feng Wu, Xiaohao Sam Zheng, Lili Ji, Ge Yi and Jerome Marcelino

AWARDS

- 3 times Western Digital Innovative Disclosure Awards-2014-2016
- 2nd Place Graduate Student Poster Competition, 34th Annual Symposium on Applied Surface Analysis and 23rd Annual Symposium of Pacific Northwest Chapter , Richland, Washington, June 19-21, 2012
- 2nd Place Graduate Student Poster Competition, 22nd Annual Symposium of Pacific Northwest Chapter of AVS, Wilsonville, Oregon, Sept 15, 2011
- American Vacuum Society Dorothy M. and Earl S. Hoffman Travel Grant, 2010
- 3rd Place Graduate Student Poster Competition, For Student working with UHV STM/AFM, 21st Annual Symposium of Pacific Northwest Chapter of AVS, Richland, Washington, Sept, 16, 2010